RHEUMATOLOGY
QUARTERLY

RQ

Rheumatology Quarterly

galenos
yayınevi

September
2024

Please refer to the journal's webpage (**https://qrheumatol.com/**) for "Aims and Scope", "Ethical Policy", "Instructions to Authors" and "Instructions to Reviewers".

The editorial and publication processes of the journal are shaped in accordance with the guidelines of the ICMJE, WAME, CSE, COPE, EASE, and NISO. Rheumatology Quarterly is indexed in **EBSCO Host Research Databases** and **Gale/Cengage Learning**.

The journal is published online.

Owner: Galenos Publishing House

Responsible Manager: Sekib Sokolovic

RQ
Rheumatology Quarterly

CONTENTS

AN OVERVIEW OF JANUS KINASE INHIBITORS

Ⓘ Fatih Albayrak

Dr. Ersin Arslan Training and Research Hospital, Clinic of Rheumatology, Gaziantep, Turkey

Abstract

With a better understanding of the pathogenesis of inflammatory rheumatic diseases, different treatments pathways have emerged. In recent years, Janus kinase inhibitors (JAKinibs) have become one of these treatment pathways. It has come into clinical use as an effective treatment agent, especially in rheumatoid arthritis and spondyloarthropathy. In the 21st-century, experimental and clinical studies are being conducted on JAKinibs in different disease groups apart from rheumatological diseases around the world. In this review, we aimed to briefly discuss the historical development and clinical use of JAKinibs.

Keywords: Janus kinase inhibitor, rheumatological diseases, history

INTRODUCTION

There are many reasons for the pathogenesis of rheumatic diseases. Many environmental, epigenetic, genetic, and cellular causes may be involved in the pathogenesis of diseases. When we look at the genetic causes, some mutations, translocation of some genetic regions in DNA gene sequence, overexpression, and irregularities in intracellular protein kinase activation play an important role in the pathogenesis of autoimmune diseases, inflammatory rheumatic, neuropsychiatric, cardiovascular diseases, and malignancies.

Since the beginning of the 21st century, with a better understanding of the pathogenesis of rheumatic diseases, new generation treatment agents that act at the level of many targeted receptors and cytokines have been added to the conventional treatment agents that we use today. Treatment agents that act especially at the protein kinase level constitute the most important treatment agents in the 21st century (1,2).

Perhaps 25-33% of drug development efforts in the United States of America (USA) and around the world target these enzymes (3).

Brief History of JAKs and their Mechanism of Action

Protein kinases control metabolism, transcription, cell division, movement, and programed cell death. Protein phosphorylation provides a balance between phosphoprotein kinases and protein kinases that perform reversible phosphorylation-dephosphorylation functions in the cell (4,5). Because of the general importance of protein phosphorylation, significant efforts have been made to identify the various functions of protein kinase signal transduction pathways. Inflammatory rheumatic diseases and malignances may occur because of derangements in the activation of protein kinase.

From this perspective, the first protein kinase inhibitor was developed by Hidaka et al. (6) in 1980. Isoquinoline sulfonamide was shown to inhibit protein kinase in 1984. However, protein kinase inhibition did not enter clinical trials until the late

1980s. Toward the end of the 1990s, pharmaceutical companies began to study protein kinase inhibition. In these years, the three-dimensional form of protein kinase has been shown. Cyclosporine inhibits protein phosphatase, whereas rapamycin inhibits protein kinase (7). The first protein kinase inhibitor (Fasudil) was used for treating cerebral ischemia in Japan (8,9). Following this development, the imatinib molecule began to take part in clinical trials in chronic myeloid leukemia (CML) in 1996 and was accepted as a treatment option in CML in 2001 in the USA. On the other hand, rapamycin entered clinical use in USA as an immunosuppressive therapy in 1999 (10).

Cytokine binding to these receptors activates phosphotransferases (kinases) associated with the intracellular part of these receptors. These kinases belong to a small family called Janus kinase (JAK), which consists of four members: JAK1, JAK2, JAK3, and tyrosine kinase (TYK)2. Different receptors are coupled with different JAKs working in pairs in a heterodimeric or homodimeric complex. JAKs are intracellular enzymes that are activated by the binding of cytokines to cell surface receptors. Following receptor binding, JAKs phosphorylate themselves and tyrosine residues on the receptor chains that recruit the signal transducers and activators of transcription of DNA-binding proteins. These factors are phosphorylated by JAKs, resulting in dimerization, translocation to the nucleus, and subsequent regulation of gene expression. A number of mutant cell lines revealed the essential functions of JAKs in cytokine signaling. However, identification of JAK3 mutations in patients with severe combined immunodeficiency revealed criticality *in vivo*, as in various knockout mice (11,12). These considerations led to the suggestion that JAK inhibitors could be used as a new immunomodulatory drug therapy (13). Recognition of JAK2 gain-of-function (GOF) mutations in MPN provides further evidence of JAK inhibition as an attractive therapeutic option (14). In humans, mutation of TYK2 causes primary immunodeficiency (15). TYK2 is associated with systemic lupus erythematosus and Crohn's disease (16,17) and JAK2 polymorphisms are associated with Behçet's disease (18). Considering the role of cytokines in autoimmunity, inhibition of JAK blocks the effects of many cytokines and appears as an alternative treatment option for some diseases. The rationale for targeting JAKs derives from the vast amount of data demonstrating the role of cytokines in autoimmune disease, the success of biologics, and conclusive evidence of the necessary role of JAKs in cytokine signaling both *in vitro* and *in vivo*. JAK1 blockade inhibits signaling by interferon (IFN)-α, IFN-gamma, interleukin (IL)-6 , and others Blockade of JAK2 reduces the signaling of IL-3, IL-5, and IFN-gamma and reduces the hematopoietic growth factor erythropoietin, thrombopoietin, and granulocyte macrophage colony-stimulating factor. On the other hand, JAK3 blockade interferes with the effects of IL-2, IL-4, IL-15, IL-21, and other cytokines (19).

Clinical use of JAKs

Tofacitinib: Tofacitinib is the first Jakinib drug developed for autoimmune diseases. It inhibits JAK1 and JAK3 and, to a lesser extent, inhibits JAK2 (20). After promising results in preclinical and early phase clinical trials, it was extensively evaluated in key studies in 2012 (21). Multiple phase 2 and phase 3 studies demonstrated the efficacy of tofacitinib when used as monotherapy or in combination with other disease-modifying antirheumatic

drug (DMARD) treatment agents for rheumatoid arthritis (RA) (22,23). Later, it entered clinical use for treating psoriatic arthritis (PsA) (24) and was subsequently approved for clinical use for treating ulserative colitis (25).

Baricitinib: As a JAK1/JAK2 inhibitor, it has been approved in the USA for patients with RA limited to 2 mg per day in combination with a conventional synthetic DMARD (csDMARD) or as monotherapy in patients with RA who are resistant to a biological

DMARDs (bDMARDs) based on phase 3 trial results. In other countries, it has been approved for clinical use as 2 and 4 mg in patients resistant to csDMARD (26,27). In addition, it has been approved for use for treating atopic dermatitis in Europe.

Peficitinib: Peficitinib is a pan Jakinib that has been approved for use for treating RA in Japan, South Korea, and Taiwan (28,29).

Upadacitinib: The second generation selective JAK inhibitor upadacitinib has a selective and potentially more pronounced inhibitory effect on JAK1 than the other subtypes. Phase 3 trials demonstrated clinical, functional, and radiographic efficacy, both along with a csDMARD and as monotherapy, in patients who did not respond completely to a csDMARD or bDMARD (30,31). It has also been approved for spondylitis and PsA (32,33) and is effective in inflammatory bowel disease.

Filgotinib: Filgotinib is a second-generation JAK1 inhibitor that has recently been approved for clinical use in Europe (33). *In vitro* selective JAK 1 inhibitors, such as upadasitinib, but clinical and safety measures are similar to pan JAKinibs, but herpes zoster and anemia are less frequent with filgotinib treatment.

Ruxolitinib: Ruxolitinib, a JAK1/JAK2 inhibitor, was the first agent to be approved for myeloproliferative neoplasms (MPN) that frequently display GOF JAK2 mutations. It has also been approved for steroid-resistant acute graft-versus-host disease (GvHD).

Fatih Albayrak. An Overview of Janus Kinase Inhibitors

Rheumatology Quarterly 2024;2(3):98-101

Oclacitinib: Oclacitinib is a non-selective JAKinib approved for treating eczema in dogs.

Side effect profile of JAKinibs: Although jakinib treatments have similar side effects as other bDMARD treatments, some side effects are different. Common side effects include infection, serious and opportunistic infections, and herpes zoster. Cytopenias such as neutropenia and anemia are also common adverse events, likely due to JAK2 inhibition. Upadacitinib, a relatively JAK1-selective molecule, has similar effects as pan-JAKinibs on anemia, whereas filgotinib appears to produce less anemia. JAKinibs can also cause lymphopenia, specifically a decrease in natural killer cells due to the JAK3 inhibitor.

There is an increased risk of pulmonary thromboembolism and deep vein thrombosis complications in patients with RA, and it seems difficult to associate this complication with a cytokine pathway. JAK2 inhibition may impair thrombotic haemoastasis, but this side effect may be associated with the comorbidity of some non-target treatment comorbid conditions.

From the point of view of malignancy, it is important to use JAKinibs in some solid and hematological malignancies other than rheumatological diseases. The use of this group of drugs in other rheumatological diseases, especially in RA, does not increase the risk when compared with other treatment agents and has been safely used for many years.

CONCLUSION

In recent years, approximately 180 protein kinase inhibitors have been used in clinical trials worldwide, and there are 72 FDA-approved protein kinase inhibitors. JAKinibs have started to be used for treating many rheumatic diseases. Ral use in particular is an advantage and is important in terms of patient compliance. In terms of side effects, long-term results should be closely monitored. It seems that more Jakinib will be used in clinical use in the coming years.

Footnote

REFERENCES

1. Cohen P. Protein kinases-the major drug targets of the twenty-first century? Nat Rev Drug Discov. 2002;1:309-15.

2. Roskoski R Jr. A historical overview of protein kinases and their targeted small molecule inhibitors. Pharm Res. 2015;100:1-23.

3. Roskoski R Jr. Properties of FDA-approved small molecule protein kinase inhibitors: a 2023 update. Pharmacological Res. 2023;187:106552.

4. Manning G, Whyte DB, Martinez R, et al. The protein kinase complement of the human genome. Science. 2002:1912-34.

5. Alonso A, Sasin J, Bottini N, et al. Protein tyrosine phosphatases in the human genome. Cell. 2004;11;117:699-711.

6. Hidaka H, Inagaki M, Kawamoto S, et al. Isoquinolinesulfonamides, novel and potent inhibitors of cyclic nucleotide dependent protein kinase and protein kinase C. Biochemistry. 1984;9;23:5036-41.

7. Liu J, Farmer JD Jr, Lane WS, et al. Calcineurin is a common target of cyclophilin-cyclosporin A and FKBP-FK506 complexes. Cell. 1991;23;66:807-15.

8. Shibuya M, Suzuki Y, Sugita K, et al. Effect of AT877 on cerebral vasospasm after aneurysmal subarachnoid hemorrhage. Results of a prospective placebo-controlled double-blind trial. J Neurosurg. 1992;76:571-7.

9. Asano T, Ikegaki I, Satoh S, et al. A protein kinase inhibitor, fasudil (AT-877); a novel approach to signal transduction therapy. Cardiovascular Drug Rev. 1998:76-87.

10. Davies SP, Reddy H, Caivano M, et al. Specificity and mechanism of action of some commonly used protein kinase inhibitors. Biochem J. 2000;1;351:95-105.

11. Darnell JE Jr, Kerr IM, Stark GR. Jak-STAT pathways and transcriptional activation in response to IFNs and other extracellular signaling proteins. Science. 1994;264:1415-21.

12. Russell SM, Tayebi N, Nakajima H, et al. Mutation of Jak3 in a patient with SCID: essential role of Jak3 in lymphoid development. Science. 1995;270:797-800.

13. Changelian PS, Flanagan ME, Ball DJ, et al. Prevention of organ allograft rejection by a specific Janus kinase 3 inhibitor. Science. 2003;302:875-8.

14. Kralovics R, Passamonti F, Buser AS, et al. A gain-of-function mutation of JAK2 in myeloproliferative disorders. N Engl J Med. 2005;352:1779-90.

15. Kreins AY, Ciancanelli MJ, Okada S, et al. Human TYK2 deficiency: Mycobacterial and viral infections without hyper-IgE syndrome. J Exp. Med 2015;212:1641-62.

16. Sigurdsson S, Nordmark G, Göring HH, et al. Polymorphisms in the tyrosine kinase 2 and interferon regulatory factor 5 genes are associated with systemic lupus erythematosus. Am J Hum Genet. 2005;76:528-37.

17. Franke A, McGovern DP, Barrett JC, et al. Genome-wide meta-analysis increases to 71 the number of confirmed Crohn's disease susceptibility loci. Nat Genet. 2010; 42:1118-25.

18. Hu K, Hou S, Jiang Z, et al. JAK2 and STAT3 polymorphisms in a Han Chinese population with Behcet's disease. Invest Ophthalmol Vis Sci. 2012; 53:538-41.

19. O'Shea JJ, Schwartz DM, Villarino AV, et al. The JAK-STAT pathway: impact on human disease and therapeutic intervention. Annu Rev Med. 2015;66:311-28.

20. Fleischmann R, Kremer J, Cush J, et al. Placebo-controlled trial of tofacitinib monotherapy in rheumatoid arthritis. N Engl J Med. 2012;367:495-507.

21. Lee EB, Fleischmann R, Hall S. Radiographic, clinical and functional comparison of tofacitinib monotherapy versus methotrexate in

methotrexate-naïve patients with rheumatoid arthritis. Arthritis Rheum. 2012;64:S1049.

22. Gladman D, Rigby W, Azevedo VF, et al. Tofacitinib for psoriatic arthritis in patients with an inadequate response to TNF inhibitors. N Engl J. Med 2017;377:1525-36.

23. Sandborn WJ, Su C, Panes J. Tofacitinib as Induction and maintenance therapy for ulcerative colitis. N Engl J Med. 2017;377:496-7.

24. Genovese MC, Kremer J, Zamani O, et al. Baricitinib in patients with refractory rheumatoid arthritis. N Engl J Med. 2016;374:1243-52.

25. Dougados M, van der Heijde D, Chen YC, et al. Baricitinib in patients with inadequate response or intolerance to conventional synthetic DMARDs: results from the RA-BUILD study. Ann Rheum Dis. 2017;76:88-95.

26. Tanaka Y, Takeuchi T, Tanaka S, et al. Efficacy and safety of peficitinib (ASP015K) in patients with rheumatoid arthritis and an inadequate response to conventional DMARDs: a randomised, double-blind, placebo-controlled phase III trial (RAJ3). Ann Rheum Dis. 2019;78:1320-32.

27. Takeuchi T, Tanaka Y, Tanaka S, et al. Efficacy and safety of peficitinib (ASP015K) in patients with rheumatoid arthritis and an inadequate response to methotrexate: results of a phase III randomised, double-blind, placebo-controlled trial (RAJ4) in Japan. Ann Rheum Dis. 2019;78:1305-19.

28. Genovese MC, Fleischmann R, Combe B, et al. Safety and efficacy of upadacitinib in patients with active rheumatoid arthritis refractory to biologic disease modifying anti-rheumatic drugs (SELECT-BEYOND): a double-blind, randomised controlled phase 3 trial. Lancet. 2018;391:2513-24.

29. Burmester GR, Kremer JM, Van den Bosch F, et al. Safety and efficacy of upadacitinib in patients with rheumatoid arthritis and inadequate response to conventional synthetic disease-modifying anti-rheumatic drugs (SELECT-NEXT): a randomised, double-blind, placebo-controlled phase 3 trial. Lancet. 2018;391:2503-12.

30. McInnes IB, Kato K, Magrey M, et al. Upadacitinib in patients with psoriatic arthritis and an inadequate response to non-biological therapy: 56- week data from the phase 3 SELECT-PsA 1 study. RMD Open. 2021;7:e001838.

31. White JPE, Coates LC. JAK1 selective inhibitors for the treatment of spondyloarthropathies. Rheumatology. 2021;60:ii39-ii44.

32. Harris C, Cummings JRF. JAK1 inhibition and inflammatory bowel disease. Rheumatology. 2021;60:ii45-ii51.

33. European Medicines Agency. Filgotinib (Jyseleca): EU summary of product characteristics. 2020.

A REVIEW OF BARICITINIB: EFFICACY AND SAFETY IN RHEUMATIC DISEASES

Ⓘ Ayten Yazıcı, Ⓘ Senar Şan

Kocaeli University Faculty of Medicine, Department of Internal Medicine, Division of Rheumatology, Kocaeli, Turkey

Abstract

Baricitinib is an oral Janus kinase (JAK) inhibitor and a member of the targeted synthetic disease-modifying anti-rheumatic drugs. Baricitinib competitively binds to adenosine triphosphate and inhibits the synthesis of cytokines that play prominent roles in arthritis rheumatoid arthritis pathogenesis by selectively inhibiting JAK1 and JAK2 at an effective dose. Its bioavailability is approximately 80%, and 64% is excreted via the kidney. To evaluate the efficacy and safety of baricitinib, 19 clinical pharmacological studies and 3 phase II, 4 phase III, and one extension study were conducted in patients with rheumatoid RA. The effectiveness of baricitinib has been shown in these studies. Clinical research and real-world data suggest that baricitinib is a safe drug; however, it has been reported to have some well-known side effects such as neutropenia, anemia, elevation of transaminase levels, hyperlipidemia, and increased risk of infections. In these studies, major cardiovascular events were found to be similar in frequency to placebo, and the incidence of malignancy was found to be similar to that of age-related cancer in the general population. However, as is the case with other JAK inhibitors, it is recommended to be used with caution in patients with risk factors for deep vein thrombosis, such as advanced age, obesity, and inactivity.

Keywords: Janus kinase, baricitinib, rheumatoid arthritis, disease-modifying anti-rheumatic drug

INTRODUCTION

As the roles of cytokines and the pathophysiological pathways of autoimmune diseases have become clearer, new therapeutic agents have been introduced. Among these agents, Janus kinase (JAK) inhibitors have been approved by the Food and Drug Administration (FDA) for the treatment of rheumatoid arthritis (RA) and have been added to the treatment guidelines as second-line therapy.

JAK is a member of the intracellular tyrosine kinase (TYK) family and plays an important role in the signaling pathways of proinflammatory cytokines involved in the pathogenesis of inflammatory and autoimmune diseases. Participating in the signal transduction of Type I and Type II cytokine receptors, this intracellular molecule has 4 different isoforms, JAK1, JAK2, JAK3, and TYK2. These isoforms usually exist as dimers and are responsible for the phosphorylation of other intracellular proteins. Different cytokines use different dimers, and autophosphorylation of JAKs occurs when cytokines bind to receptors on the cell surface. Activated JAKs induce gene transcription and cytokine synthesis by phosphorylating intracellular proteins signal transducers and activators of transcription (STAT) (1,2).

JAK inhibitors are classified by European League Against Rheumatism as targeted synthetic disease-modifying anti-

Address for Correspondence: Ayten Yazıcı, Kocaeli University Faculty of Medicine, Department of Internal Medicine, Division of Rheumatology, Kocaeli, Turkey

Phone: +90 262 303 75 25 **E-mail:** burakdefy@hotmail.com **ORCID ID:** orcid.org/0000-0003-2167-4509

rheumatic drug (DMARDs). Of these agents, tofacitinib, baricitinib and upadacitinib are FDA-approved for the treatment of RA. Each JAK inhibitor binds to these receptors with varying selectivity. Tofacitinib inhibits JAK1/3, baricitinib inhibits JAK1/2 and upadacitinib inhibits JAK1 selectively (Figure 1) (1-3).

Methotrexate (MTX) is the gold standard treatment in RA and is recommended as first-line therapy (4,5). Patients who do not respond to this treatment are considered MTX-resistant, and it is recommended to switch to second-line therapy in these patients. Treatment guidelines include biological (b) DMARDs and targeted synthetic DMARDs as second-line therapy. Generally, combination therapy is administered in RA, but MTX treatment is discontinued in one-third of patients due to drug intolerance. In such cases, bDMARDs and JAK inhibitors, which can also be used as monotherapy, stand out as alternative treatment options (4,6).

The first JAK inhibitor, tofacitinib, was approved by the FDA in 2009. In 2017, baricitinib was approved in Europe alongside tofacitinib. Baricitinib competitively binds to the adenosine triphosphate (ATP)-binding site of JAK and blocks phosphate

transfer from ATP to JAK, thereby inhibiting JAK activation and JAK/STAT phosphorylation and consequently inhibiting cytokine synthesis. The activation of the JAK1 and JAK2 signaling pathway leads to the synthesis of interleukin (IL)-6, IL-23, granulocyte colony-stimulating factor, granulocyte-macrophage colony-stimulating factor, interferon, and erythropoietin, which play prominent roles in RA pathogenesis. Baricitinib inhibits the synthesis of all these cytokines by selectively inhibiting JAK1 and JAK2 at an effective dose (2).

Oral baricitinib (4 mg) is rapidly absorbed after administration and reaches peak plasma concentration in 1.5 hours. Because its half-life is around 14 hours, it is recommended to be used once daily. Bioavailability is approximately 80%. While 64% is excreted via the kidney without being metabolized, 15% is excreted through the feces. Because of its high renal excretion, a dose reduction is recommended if creatinine clearance is 30-60 mL/min, whereas it is not recommended as a therapeutic option if creatinine clearance is below 30 mL/min. Its absorption is not affected by meals or using it with drugs that affect gastric pH, such as omeprazole. However, it acts as a substrate for many
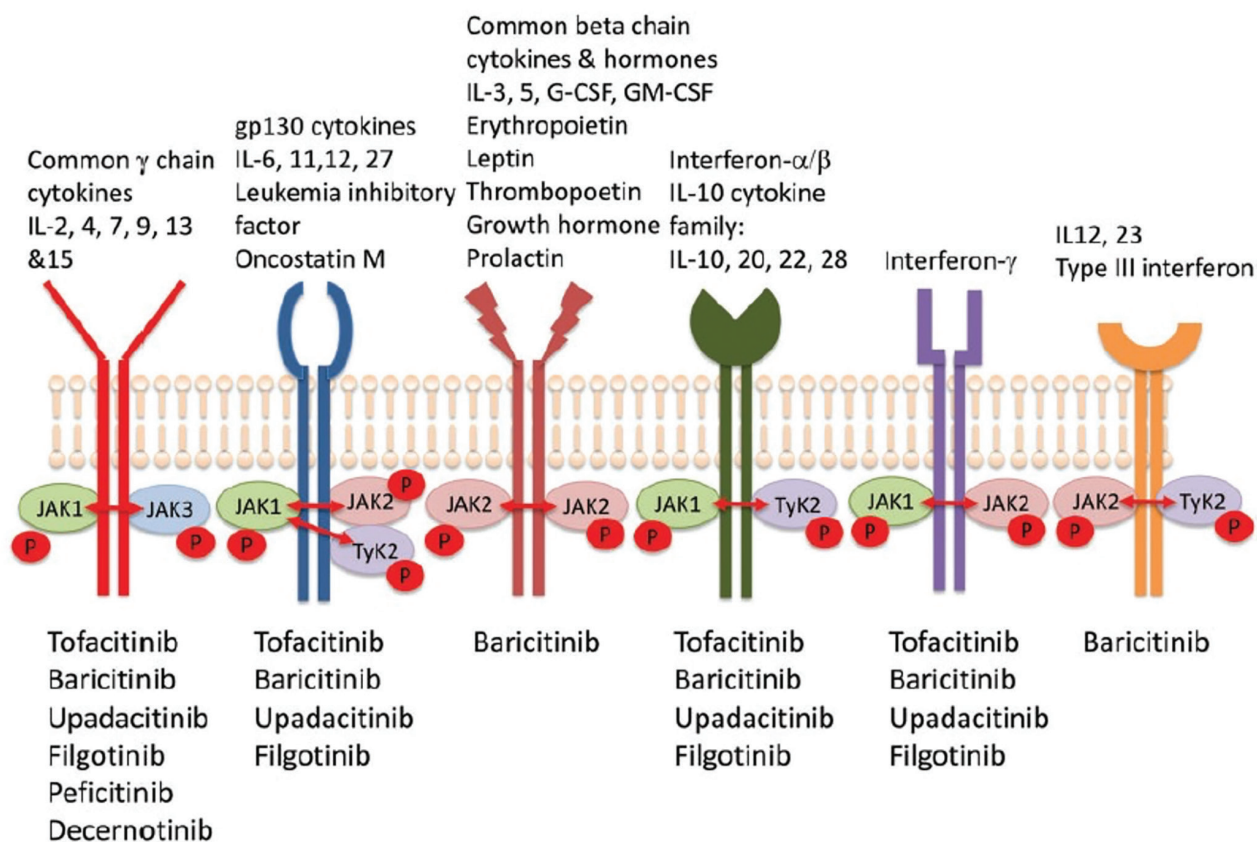

Figure 1. Relationship between JAK inhibitors and cytokines (2)
JAK: Janus kinase, IL: Interleukin, G-CSF: Granulocyte colony-stimulating factor, GM-CSF: Granulocyte-macrophage colony-stimulating factor

Yazıcı and Şan. The Efficacy and Safety of Baricitinib

Rheumatology Quarterly 2024;2(3):102-7

renal transporter proteins and may theoretically affect the plasma concentration of drugs such as probenecid, ibuprofen, diclofenac, and leflunomide. In addition, it is recommended to limit the baricitinib dose so that it does not exceed 2 mg daily in patients using probenecid (2).

Efficacy Data

To evaluate the efficacy and safety of baricitinib, 19 clinical pharmacological studies and 3 phase II, 4 phase III, and one extension study were performed. One of the phase III studies, RA-BEGIN, compared 4 mg/day baricitinib with MTX in bDMARD-naive patients with early RA. In this study, it was shown that both baricitinib monotherapy and combination therapy with MTX were superior to MTX monotherapy in terms of efficacy at week 12, and the efficacy was sustained until week 52. In the RA-BEAM study, baricitinib (4 mg) was compared with adalimumab (40 mg) in MTX-resistant RA patients, and American College of Rheumatology (ACR) response at week 12 (70% vs 61%; p=0.014) and the change in disease

activity score 28-C-reactive protein (DAS28-CRP) (-2.24 vs -1.95; p<0.001) were greater in the baricitinib group. This study also emphasized that there was greater improvement in several quality-of-life indices in baricitinib recipients compared with those on placebo and adalimumab, and that this efficacy was sustained for 52 weeks (2,7-9).

In a meta-analysis of MTX-resistant patients, Fakhouri et al. (5) found that the baricitinib-MTX combination was superior to the combination of MTX with other bDMARDs (adalimumab, abatacept, rituximab, infliximab, tocilizumab) in terms of ACR20 and ACR70 responses at week 24, but there was no difference between the two groups in terms of ACR50 responses. No significant superiority was found against the tofacitinib-MTX combination (5).

In a phase III study investigating the efficacy of baricitinib in patients with RA who were resistant to bDMARDs (RA-BEACON), responses to placebo and baricitinib were compared. The authors noted an ACR20 response of 55% for baricitinib and 27% for placebo at week 12 (p<0.001). It was also reported that changes in DAS28-CRP and health assessment questionnaire-disability index scores favored baricitinib (10).

In the RA-BEGIN study, ACR20 responses at week 24 were 77% with baricitinib monotherapy and 62% with MTX monotherapy (p≤0.01). In the same study, structural damage at week 52 was also evaluated, and the odds ratio was 0.62 [95% confidence interval (CI): 0.35, 1.09] in baricitinib monotherapy and 0.39 (95% CI: 0.22-0.70) in combination therapy compared with MTX. It was emphasized that there was a lower likelihood of

progression regarding structural damage in patients without a permanent clinical response to the baricitinib-MTX combination and that progression was associated with high hs-CRP, high clinical disease activity index score, female sex, smoking history, and lower body mass index (8,11). Radiological response was evaluated in the RA-BEAM and RA-BUILD studies, and baricitinib was found to significantly prevent the progression of structural joint damage (2,8).

Real-world data from an Italian study of 446 RA patients (34% bDMARD-naive and 66% bDMARD-resistant) treated with baricitinib 4 mg showed a remission rate of 64% and low disease activity rate of 17% at 12 months, with a superior clinical response in the bDMARD-naive group. In this study, it was also emphasized that oral glucocorticoid treatment could be discontinued in 50% of patients in the first year. It was also reported that 24% of patients discontinued treatment because of ineffectiveness and 13% because of side effects, and that the risk of discontinuation because of ineffectiveness was lower in patients with rheumatoid factor and cyclic citrullinated peptide positivity or bDMARD-naive patients (12). With real-world data from Japan (n=4731), it was observed that 24.8% of patients stopped taking the drug before week 24, and the reason for discontinuation in most of the cases (10.1%) was reported to be ineffectiveness (13). In a 9.3-year study comparing baricitinib treatment as monotherapy or in combination with MTX, there was no difference in drug continuation at week 96 between monotherapy (62%) and MTX combination (56%). In this study, it was reported that 30.1% of patients discontinued treatment due to ineffectiveness and 8.6% discontinued treatment due to side effects (14). In a study including 19 different country databases, JAK inhibitors users (41% baricitinib, 59% tofacitinib) were less likely to discontinue because of ineffectiveness and more likely to discontinue because of side effects compared with tumor necrosis factor inhibitors users (15).

Safety Data

Clinical research and real-world data suggest that baricitinib is a safe drug; however, it has been reported to have many effects on laboratory parameters besides its established side effects. Hemograms showed a decrease in neutrophil count in the first month and a return to baseline values after treatment discontinuation. Neutropenia (<1000/mm^3) is rare (<1% of patients) and has not been associated with serious infection. It was reported that lymphocyte count increased in the first month and returned to baseline levels at follow-up. A relationship between lymphopenia and the risk of infection was noted, but this did not appear to increase the likelihood of serious infections. Although

Rheumatology Quarterly 2024;2(3):102-7

Yazıcı and Şan. The Efficacy and Safety of Baricitinib

a decrease in platelet count was expected considering the effect of the JAK-2 pathway on thrombopoietin, an increase in platelet count was observed. The platelet count reached baseline levels at week 2 of treatment and remained stable. No significant relationship was found between the thrombocytosis experienced during this period and the potential development of pulmonary embolism (PE)/deep vein thrombosis (DVT). Although a decrease in hemoglobin level is observed at the beginning of treatment because of its effects on erythropoietin, this effect is transient and levels have been reported to return to baseline levels within a short period. Drug discontinuation due to anemia is rare, and the frequency of cases where hemoglobin levels fall below 8 mg/dL is less than 1% (2,7). Nonetheless, it is recommended to discontinue treatment if the absolute neutrophil count is below 1000/mm^3, if the absolute lymphocyte count is below 500/mm^3, and if the hemoglobin level is below 8 mg/dL during baricitinib treatment, and to resume treatment only when laboratory values return to normal (2).

Various changes in the lipid profile have also been reported with baricitinib. Although there was an average increase of 9.5 mg/dL in low density lipoprotein (LDL) cholesterol, 7.3 mg/dL in high density lipoprotein (HDL) cholesterol and 8.5 mg/dL in triglyceride levels, the LDL/HDL ratio did not change and these values reached a plateau at week 12 and remained stable thereafter. Creatinine levels increased by an average of 3.8 μmol/L at week 2 after the initiation of treatment and it was noted that a slight decrease in glomerular filtration rate may develop without loss of renal function. In addition, elevated alanine aminotransferase and aspartate aminotransferase levels were detected in 1.9% and 1.3% of barictinib monotherapy recipients, respectively, and these elevations in liver function tests were transient in most cases (2,7). However, hepatic dysfunction with a rate of 2.77% during the 24-week follow-up was also reported in a Japanese cohort (13).

During the 24-week follow-up in the RA-BEACON study, side effects were reported in 64% of the placebo group, 71% of the baricitinib 2 mg group, and 77% of the baricitinib 4 mg group. The rate of serious side effects was 7% in the placebo group, 4% in the baricitinib 2 mg group, and 10% in the baricitinib 4 mg group, and the serious infection rates were 3%, 2%, and 3%, respectively. Although herpes zoster (HZ) infections were observed in all groups, they were most common in the baricitinib 4 mg group (4%). None of the groups demonstrated disseminated HZ involvement or organ involvement (10). When the safety data of 9 studies on baricitinib were analyzed, the frequency of serious infections was found to be similar to placebo in a 5.5-year follow-up of 3492 patients, with the most commonly observed

serious infections being pneumonia (0.5/100 patient-years), HZ infection (0.4/100 patient-years), urinary tract infection (0.3/100 patient-years), and cellulitis (0.1/100 patient-years). Tuberculosis was reported in only 10 cases, and it was emphasized that these subjects were living in countries with high tuberculosis incidence (2,8,16). In a systematic review of tuberculosis cases associated with JAK inhibitors, the incidence of tuberculosis was reported to be 0.28% (79/28099) with tofacitinib and 0.23% (10/4310) with baricitinib (17).

Looking at the frequency of adverse events in real-world data, adverse events were found to have occurred in 26.87% of patients, whereas serious adverse events occurred in 4.29% of patients during a 24-week follow-up in the Japanese cohort (n=4731). In this cohort, where 54% of the patients were 65 years and older, the frequency of serious infection and HZ were 1.90% and 3.09%, respectively (13). In a database study from Italy, it was observed that within 1 year, 13% of patients discontinued treatment because of side effects, and it was emphasized that the frequency of discontinuation because of side effects was higher, especially in elderly patients and in the bDMARD-resistant patient group [hazard ratio (HR): 1.03, 95% CI: 1.01-1.06; p=0.008 and HR: 1.93, 95% CI: 1.01-3.67; p=0.045, respectively] (12).

When the safety data of 9 studies on baricitinib were evaluated, the frequency of serious adverse events, including death, was 9/100 and the mortality rate was 0.33/100 patient-years in a 5.5-year follow-up of 3492 patients (2). Long-term data from these 9 studies revealed an exposure-adjusted incidence rate (EAIR) of 0.56 for death. Of the 85 deaths, 22.4% were related to cardiovascular events, 22.4% to infection, 22.4% to malignancy, and 15% to respiratory problems, irrespective of the dosage (16). In the Japanese cohort of 4731 patients, mortality was reported to be 0.38% (13).

Major cardiovascular events (MACE) were similar in frequency to placebo, and there was no data that barictinib aggravated heart failure (2). The data of all studies over a period of 9.3 years showed incidence rates of 0.5 for MACE, 0.35 for DVT, and 0.49 for DVT/PE, and these rates remained stable over time. When patients with PE and DVT were analyzed, it was found that these patients had risk factors such as DVT history, family history, hypertension, chronic obstructive pulmonary disease, pulmonary fibrosis, and varicose veins (2,16). In a Japanese cohort of 4731 patients, MACE and venous thromboembolism were similarly reported to be detected in 0.15% of patients (13).

There were 3 malignancy cases in the RA-BEAM study, whereas there was one malignancy in each of the RA-BUILD and RA-BEGIN studies. The incidence of malignancy in extension studies was similar to that in placebo (baricitinib 0.5/100 patient-years,

Yazıcı and Şan. The Efficacy and Safety of Baricitinib

Rheumatology Quarterly 2024;2(3):102-7

placebo 0.5/100 patient-years) (2,8). The long-term data from 9 studies on baricitinib showed that pulmonary and mediastinal malignancies (n=26/EAIR: 0.17), malignancies of the breast (n=23/EAIR: 0.15), and gastrointestinal malignancies (n=19/EAIR: 0.13) were the most common malignancies. These rates were found to be similar to age-related cancer incidence in the general population (16). The malignancy rate was 0.36% within the 24-week follow-up period in the Japanese cohort (13).

In the entire baricitinib case series, diverticulosis was detected at rates similar to those in the general population, and the incidence of gastrointestinal perforation was reported to be 0.06%. It was emphasized that patients with gastrointestinal perforation had non-steroidal anti-inflammatory drugs and steroid use, and that perforation was less common than that reported with tofacitinib and bDMARDs (2,16).

The effects of baricitinib on the reproductive system have not been clearly identified, but animal studies have shown that it has teratogenic effects and a negative impact on female fertility. Severe metrorrhagia in one patient and erectile dysfunction in another patient were reported in clinical trials. As data are insufficient, baricitinib is accepted to be contraindicated during pregnancy (8).

Further Indications

JAK inhibitors are already used for treating RA and are one of the most promising therapeutic agents for many other diseases. Considering the cytokines involved in the pathogenesis of spondyloarthropathy (SpA), JAK inhibition is considered a viable therapeutic objective in PsA and AS. The following studies showing its efficacy and safety in PsA and AS, tofacitinib received FDA approval for both indications. Although there are no studies on baricitinib in SpA, a study in patients with moderate to severe psoriasis reported significant improvements in psoriasis area and severity index 50 and PASI75 scores (18-22). Moreover, there are ongoing studies on baricitinib in systemic lupus erythematosus, giant cell arteritis, alopecia areata, and chronic graft-versus-host disease (8).

CONCLUSION

In conclusion, baricitinib is a targeted drug with proven efficacy and safety in RA with its ease of use as a once-daily oral agent, and it is a good option in RA treatment with similar efficacy to bDMARDs. However, its side effects should be taken into consideration, as is the case with other JAK inhibitors, and it should be used with caution in patients with risk factors for DVT such as older age, obesity, immobility, or a history of DVT.

Footnote

Authorship Contributions

Design: A.Y., S.Ş., Literature Search: A.Y., S.Ş., Writing: A.Y., S.Ş.

Conflict of Interest: The authors have no conflicts of interest to declare.

Financial Disclosure: The authors declared that this study received no financial support.

REFERENCES

1. Choy EH. Clinical significance of Janus Kinase inhibitor selectivity. Rheumatology. 2019;58:953-62.

2. Choy EHS , Miceli-Richard C, González-Gay MA, et al. The effect of JAK1/JAK2 inhibition in rheumatoid arthritis: efficacy and safety of baricitinib. Clin Exp Rheumatol. 2019;37:694-704.

3. Wang F, Sun L, Wang S, et al. Efficacy and safety of tofacitinib, baricitinib, and upadacitinib for rheumatoid arthritis: a systematic review and meta-analysis. Mayo Clin Proc. 2020;95:1404-19.

4. Smolen JS, Landeẃe RBM, Bijlsma JWJ, et al. EULAR recom-mendations for the management of rheumatoid arthritis with synthetic and biological disease-modifying antirheumatic drugs: 2019 update. Ann Rheum Dis. 2020;79:685-99.

5. Fakhouri W, Wang X, de La Torre I, et al. A network meta-analysis to compare effectiveness of baricitinib and other treatments in rheumatoid arthritis patients with inadequate response to methotrexate. J Health Econ Outcomes Res. 2020;7:10-23.

6. Fleischmann R, Schiff M, van der Heijde D, et al. Baricitinib, methotrexate, or combination in patients with rheumatoid arthritis and no or limited prior disease-modifying antirheumatic drug treatment. Arthritis Rheumatol. 2017;69:506-17.

7. Taylor PC, Keystone EC, van der Heijde D, et al. Baricitinib versus placebo or adalimumab in rheumatoid arthritis. N Engl J Med. 2017;376:652-62.

8. Kawalec P, Śladowska K, Malinowska-Lipień I, et al. New alternative in the treatment of rheumatoid arthritis: clinical utility of baricitinib. Ther Clin Risk Manag. 2019;15:275-84.

9. Keystone EC, Taylor PC, Tanaka Y, et al. Patient-reported outcomes from a phase 3 study of baricitinib versus placebo or adalimumab in rheumatoid arthritis: secondary analyses from the RA-BEAM study. Ann Rheum Dis. 2017;76:1853-61.

10. Genovese MC, Kremer J, Zamani O, et al. Baricitinib in patients with refractory rheumatoid arthritis. N Engl J Med. 2016;374:1243-52.

11. van der Heijde D, Durez P, Schett G, et al. Structural damage progression in patients with early rheumatoid arthritis treated with methotrexate, baricitinib, or baricitinib plus methotrexate based on clinical response in the phase 3 RA-BEGIN study. Clin Rheumatol. 2018;37:2381-90.

12. Guidelli GM, Viapiana O, Luciano N, et al. Efficacy and safety of baricitinib in 446 patients with rheumatoid arthritis: a real-life multicentre study. Clin Exp Rheumatol. 2021;39:868-73.

13. Takagi M, Atsumi T, Matsuno H, et al. Safety and effectiveness of baricitinib for rheumatoid arthritis in japanese clinical practice: 24-week results of all-case post-marketing surveillance. Mod Rheumatol. 2022;roac089.

14. Bayat S, Tascilar K, Bohr D, et al. Efficacy and drug persistence of baricitinib monotherapy is similar to combination therapy I n patients with active RA: a prospective observational study. RMD Open. 2022;8:e002674.

15. Lauper K, Iudici M, Mongin D, et al. Effectiveness of TNF-inhibitors, abatacept, IL6-inhibitors and JAK-inhibitors in 31 846 patients with rheumatoid arthritis in 19 registers from the "JAK-pot"collaboration. Ann Rheum Dis. 2022;81:1358-66.

16. Taylor PC, Takeuchi T, Burmester GR, et al. Safety of baricitinib for the treatment of rheumatoid arthritis over a median of 4.6 and up to 9.3 years of treatment: final results from long-term extension study and integrated database. Ann Rheum Dis. 2022;81:335-43.

17. Cantini F, Blandizzi C, Niccoli L, et al. Systematic review on tuberculosis risk in patients with rheumatoid arthritis receiving inhibitors of Janus Kinases. Expert Opin Drug Saf. 2020;19:861-72.

18. Caso F, Navarini L, Ruscitti P, et al. Targeted synthetic pharmacotherapy for psoriatic arthritis: state of the art. Expert Opin Pharmacother. 2020;21:785-96.

19. Veale DJ, McGonagle D, McInnes IB, et al. The rationale for Janus kinase inhibitors for the treatment of spondyloarthritis. Rheumatology. 2019;58:197-205.

20. Mease PJ, Young P, Gruben D, et al. Early real-world experience of tofacitinib for psoriatic arthritis: data from a United States healthcare claims database. Adv Ther. 2022;39:2932-45.

21. Leng X, Lin W, Liu S, et al. Efficacy and safety of tofacitinib in Chinese patients with active psoriatic arthritis: a phase 3, randomised, double-blind, placebo-controlled study. RMD Open. 2023;9:e002559.

22. Papp KA, Menter MA, Raman M, et al. A randomized phase 2b trial of baricitinib, an oral Janus kinase (JAK) 1/JAK2 inhibitor, in patients with moderate-to-severe psoriasis. Br J Dermatol. 2016;174:1266-76.

JANUS KINASE INHIBITORS IN SYSTEMIC SCLEROSIS: A SCOPING REVIEW

Fatma Başıbüyük, Merih Birlik

Dokuz Eylül University Faculty of Medicine, Department of Rheumatology, İzmir, Turkey

Abstract

Systemic sclerosis (SSc) is a rare multisystemic chronic immune-mediated rheumatic disease. Although it is not common, it has the highest mortality and morbidity rate among systemic rheumatic diseases. This review aimed to analyze the results of multiple preclinical trials and clinical data on Janus kinase (JAK) inhibitors in SSc treatment and provides a comprehensive overview of JAK inhibitors as a new treatment option in SSc.

Keywords: Systemic sclerosis, JAK inhibitors, tofacitinib, baricitinib, ruxolitinib

INTRODUCTION

Systemic sclerosis (SSc) is a rare multisystemic chronic immune-mediated rheumatic disease characterized by heterogeneous manifestations of vasculopathy and fibrosis (1). Fibrosis and vasculopathy are closely related and lead to heterogeneous clinical manifestations with variable prognoses (2). Fibrosis of the skin and internal organs leads to structural deterioration and ultimately organ dysfunction. On the other hand, vasculopathy causes Raynaud phenomenon, digital ulcers, pulmonary artery hypertension, and renal crisis (2). These heterogeneous organs influence the results with considerable variability in the phenotypic manifestations, rate of disease progression, and response to therapy. Although SSc is not a common disease, it still has the highest mortality and morbidity rate among the systemic rheumatic conditions (3,4). The treatments we apply in SSc patients today are not sufficient to prevent the progression of fibrosis. Because of this, several other agents are needed for treating SSc, and recently, important breakthroughs have been made in the area of targeted therapies. Janus kinase

(JAK) proteins and the Signal Transducers and Activators of Transcription (STAT) signaling pathway are among these targets.

JAKs are members of the intracellular, non-receptor protein tyrosine kinase (TYK) family, which comprises four members: JAK1, JAK2, JAK3, and TYK2 (5). These kinases bind to transmembrane cytokine receptors and initiate signaling cascades that activate transcription factors such as STAT proteins. JAKs play a role in various physiological processes, including cell proliferation, differentiation, apoptosis, immune regulation, and hematopoiesis (6). Dysregulation of JAK activity has been implicated in the pathogenesis of various immune-mediated and inflammatory diseases and cancer (6).

The JAK-STAT pathway plays a key role in the pathogenesis of SSc by activating fibroblasts and profibrotic macrophages, which initiate the process of fibrosis through various cytokines and mediators, such as interleukin (IL)-6, tumor growth factor (TGF)-β and platelet-derived growth factor (PDGF) (7,8). Preclinical studies have shown that in SSc model mice, the JAK/STAT pathway has a crucial role in cell differentiation, extracellular matrix

remodeling, and fibrosis (9). Bellamri et al. (10) showed that ruxolitinib, a non-selective JAK inhibitor, has antifibrotic effects in the skin and lung of SSc model mice *in vivo* and in human lung fibroblasts *in vitro*. And Karatas et al. (11) showed that tofacitinib (TOFA), a potent inhibitor of JAK1 and JAK3, improves skin thickness and fibrosis in SSc model mice. These and several other *in vivo* and *in vitro* studies made it necessary to design clinical trials to show that JAK inhibitors would be beneficial for the treatment of fibrosis in SSc patients. Therefore, JAK inhibitors, which are new orally administered therapeutic agents, may prevent or slow the progression of SSc.

In this review, we provide a comprehensive overview of the preclinical and clinical trials of JAK inhibitors for SSc treatment.

Preclinical Studies of JAK Inhibitors for SSc

The exact pathogenesis of SSc has not yet been fully understood, but the main pathology involves the dysregulation of inflammation, vasculopathy, and fibrosis, which results in skin thickening and organ failure. Several studies have been conducted to elucidate the pathogenesis of SSC, and we know from recent studies that one of the target mechanisms is the JAK-STAT pathway. We already know that the JAK-STAT pathway has a key role in inflammation, and JAK inhibitors have been approved for the treatment of some inflammatory diseases such as rheumatoid arthritis (RA) and spondyloarthropathic. Recent preclinical studies showed that in SSc model mice, the JAK-STAT pathway also has a crucial role in fibrosis (9). Dees et al. (12) showed higher JAK activity in dermal fibroblasts from skin samples of SSc patients compared with healthy participants, and these results were also observed in cell cultures. To evaluate the TGF-β effect at JAK activity, they treated the healthy dermal fibroblast cultures with TGF-β. This experiment showed that treatment of healthy human dermal fibroblast cultures with TGF-β increased the JAK/STAT activity. Subsequently, they performed another study in which they treated dermal fibroblast cultures incubated with TGF-β, with JAK-2 inhibitors and they observed reduction of TGF-β target gene mRNA expression and decrease of TGF-β-induced collagen I production. On the other hand, in the healthy cultures that had not been incubated with TGF-β, the level of collagen mRNA or collagen protein did not change with JAK-2 inhibitor treatment. All these experiments showed that the JAK-STAT pathway plays an important role in the development of fibrosis, but this effect is TGF-β dependent (12). After *in vitro* studies, Dees et al. (12) established an *in vivo* bleomycin (BLM)-induced SSc mouse model and showed higher JAK activity in BLM-induced mice compared with wild-type mice. Additionally, JAK-2 inhibitors resolved dermal thickening in

BLM-induced mice, and this effect was dose dependent (12). In another study, Aung et al. (13) had BLM-induced SSc mice *in vivo* and they injected intraperitoneal TOFA (20 mg/kg) 3 times per week from days 0-28. They showed that in addition to the anti-inflammatory effects, TOFA downregulated the mRNA expression of profibrotic cytokines in both the skin and lungs.

In another study, Lescoat et al. (9) compared the anti-inflammatory and anti-fibrotic effects of three JAK inhibitors, ruxolitinib (JAK2/1 inhibitor), TOFA (JAK3/2 inhibitor), and itacitinib (JAK1 inhibitor), *in vitro* on human monocyte-derived macrophages. All three JAK inhibitors had anti-inflammatory effects by decreasing the production of pro-inflammatory cytokines in M1 macrophages, but the effect of downregulating pro-fibrotic M2 macrophages was higher with ruxolitinib and TOFA, which inhibit JAK2. In addition, ruxolitinib (JAK2/1 inhibitor) represses the upregulation of proinflammatory M1 and profibrotic M2 markers in mouse macrophages in a model of HOCl-induced interstitial lung disease (ILD) (9).

From all these preclinical studies, JAK inhibitors were considered as a targeted treatment option for SSc patients in the future.

Clinical Studies of JAK Inhibitors for SSc

In 2014, Okiyama et al. (14) showed that TOFA is effective in the prevention and treatment of mucocutaneous lesions in a CD8 T-cell-mediated model of graft-versus-host disease (GVHD) mice. In a multicenter retrospective study from Europe and the United States, in steroid-refractory acute and chronic GVHD patients, ruxolitinib was shown to be more effective in both groups compared with the other second-line therapies (15). In another study on 12 steroid-refractory sclerodermatous chronic GVHD patients treated with ruxolitinib for 1 year showed a partial improvement in skin softness in 8 of the 12 patients (16). Following the results showing that JAK inhibitors improved mucocutaneous lesions in GVHD patients, several morphea and eosinophilic fasciitis (EF) cases treated with JAK inhibitors were published. In a case series of five hypereosinophilic syndrome patients with cutaneous involvement treated with either ruxolitinib or TOFA, four of these patients had remission with one of these JAK inhibitors (TOFA or ruxolitinib) without steroid requirement (17). In addition, there have been case-based articles showing that morphea had been treated successfully with TOFA (18,19).

With respect to the fibrosing nature of morphea and EF, and the JAK inhibitors to improve the fibrosis in these two diseases, suggests they might also hold promise as a treatment option for SSc. Based on this hypothesis, several studies have been progressing to evaluate the effect of JAK inhibitors in patients with SSc.

Başıbüyük and Birlik. Janus Kinase Inhibitors in Systemic Sclerosis

Rheumatology Quarterly 2024;2(3):108-12

In a pilot trial, 66 patients with SSc were divided into two groups: 33 of them received oral TOFA 5 mg twice daily; and the remaining 33 received 10 mg weekly oral methotrexate (20). Skin thickness was assessed clinically [Modified Rodnan skin score (mRSS)] and ultrasound before the treatment and at weeks 26 and 52 in both groups. Before the treatment, median scores were similar in both groups, but in the TOFA group, significantly lower medians were observed at 26 and 52 weeks. Four severe adverse events were recorded during the trial, and one of them was in the TOFA group who developed progressive interstitial lung disease.

In another phase I/II double-blind, placebo-controlled trial, 15 early diffuse cutaneous SSc patients received TOFA (5 mg) twice a day or placebo (21). A skin biopsy was performed on each participant at the beginning and at week 12. They showed the inhibition of interferon (IFN)-regulated gene expression in SFRP2/DPP4 fibroblasts (progenitors of myofibroblasts) and in MYOC/CCL19 fibroblasts (adventitial fibroblasts) by TOFA, which targeted INF. At 24 weeks, mRSS was significantly improved in the TOFA group, and safety analysis showed no severe adverse events with TOFA.

Another pilot, single-center study was conducted in diffuse cutaneous SSc (dcSSc) patients. You compared 10 TOFA-treated patients that were all refractory to conventional immunosuppressants with 12 dcSSc patients who were all treated with cyclophosphamide (CYC) or mycophenolate mofetil (MMF) along with low or medium doses of steroids (22). All patients' baseline mRSS were similar and >10. After a 6-month follow-up, skin thickening was reassessed with mRSS, and eight TOFA-treated patients met the response criteria. One of the remaining patients' skin thickening was improved as well; however, it did not meet the criteria. The last one did not respond to the treatment. When compared with CYC/MMF-treated patients, mRSS significantly improved after TOFA treatment. There were no severe adverse events in TOFA-treated patients.

In a case report from the University of Tokyo, Komai et al. (23) treated a SSc patient suffering from polyarthritis who had been previously treated with methotrexate, abatacept, and tocilizumab with TOFA 5 mg daily. During treatment, at day 28, along with a decrease in the patient's Disease Activity Score 28, they also observed a significant improvement in nailfold capillary findings and mRSS.

There are also much case-based review data in the literature. Moriana et al. (24) analyzed these data to evaluate the efficacy and safety of JAK inhibitors in SSc patients. They analyzed 59 patients from clinical trials and case reports, including some trials mentioned above. Among these 59 patients, 47 were treated with TOFA, and 12 with barricitinib. The analysis showed that 52 patients had significant cutaneous response and twenty eight of 31 ILD patients did not experience progression after treatment with TOFA. Only two patients had worsened, one with skin fibrosis and the other with ILD. In addition, no severe adverse events were described in these 59 patients.

Safety

Currently, five JAK inhibitors, TOFA (JAK1/3), baricitinib (JAK1/2), peficitinib (pan-JAK), upadacitinib (JAK1), and filgotinib (JAK1), have been approved for rheumatoid arthritis treatment, and they have been approved in phase 3 clinical trials for other diseases, such as psoriatic arthritis, ankylosing spondylitis, and axial spondyloarthritis.

In 2012, after TOFA was approved by the Food and Drug Administration (FDA), the agency designed a post-marketing clinical trial, the ORAL Surveillance. ORAL Surveillance was the FDA-mandated post-marketing phase IIIb-IV study, which enrolled 4,362 patients with RA aged >50 years who had at least one cardiovascular risk factor (25). As a result, major adverse cardiovascular events and cancers occurred more often with TOFA than with a tumor necrosis factor inhibitors (TNFi) in this trial that included patients with RA who were 50 years of age or older and had at least one additional cardiovascular risk factor. This analysis also revealed a higher risk of no serious infections and herpes zoster with TOFA versus TNFi and a higher risk of serious infections with TOFA 10 mg two times per day versus TNFi, particularly in patients aged ≥65 years (26).

After ORAL Surveillance, FDA alerted on JAK inhibitors and there had been several clinical trials with TOFA and other JAK inhibitors, but they showed that the risk of malignancy and cardiovascular events was similar with the TNFi in contrast to ORAL Surveillance (27). All trials have mentioned JAK inhibitors with good safety profiles. However, further studies are needed.

In SSc, JAK inhibitors seem to be an optional treatment now, so there is no safety trial with JAK inhibitor treatment yet, but case-based reports showed no serious adverse events. Long- term and large clinical trials are still needed to be conducted.

DISCUSSION

Preclinical studies have shown that the JAK/STAT pathway has a crucial role in inflammation, cell differentiation, extracellular matrix remodeling, and fibrosis with various cytokines and mediators, such as IL-6, TGF-β and PDGF. Besides the anti-inflammatory effects that have been recently shown, JAK inhibitors, especially JAK2 inhibitors, improve fibrosis by decreasing the pro-fibrotic M2 macrophage marker. Preclinical

Rheumatology Quarterly 2024;2(3):108-12

Başıbüyük and Birlik. Janus Kinase Inhibitors in Systemic Sclerosis

trials have also shown that JAK inhibitors improve skin thickness and ILD in a mouse model of SSc.

There have been several small, single-center, case-based, pilot trials and case reports on the treatment with JAK inhibitors in SSc patients. They all showed that JAK inhibitors improved skin thickening, arthritis, and ILD symptoms in SSc patients. There had been no severe adverse events observed in these JAK inhibitor-treated SSc patients.

It is already recognized that SSc is a chronic multisystemic disease with heterogeneous manifestations by different pathological conditions such as vasculopathy, inflammation, and fibrosis, but the exact pathogenesis remains unknown. Therefore, the treatments we apply in SSc patients today are not sufficient to prevent progression of fibrosis. SSc still has a high mortality and morbidity rate.

However, these preclinical trials showed that because of the different multiple pathological conditions such as vasculopathy, inflammation, and fibrosis play a role in SSc pathogenesis, JAK inhibitors, which play a crucial role in these pathways, may be a good option in SSc patients' treatment. In addition, the case-based trials show that JAK inhibitors work in SSc patients and it seems safe and well tolerated. Indeed, JAK inhibitors may be an effective treatment option in SSc, but more new clinical trials are needed.

Footnote

Authorship Contributions

Concept: F.B., M.B., Design: F.B., M.B., Literature Search: F.B., M.B., Writing: F.B., M.B.

Conflict of Interest: The authors have no conflicts of interest to declare.

Financial Disclosure: The authors declared that this study received no financial support.

REFERENCES

1. Volkmann ER, Andréasson K, Smith V. Systemic sclerosis. Lancet. 2023:304-18.

2. Truchetet ME, Brembilla NC, Chizzolini C. Current concepts on the pathogenesis of systemic sclerosis. Clin Rev Allergy Immunol. 2023;64:262-83.

3. Elhai M, Meune C, Boubaya M, et al. Mapping and predicting mortality from systemic sclerosis. Ann Rheum Dis. 2017;76:1897-905.

4. Steen VD, Medsger TA. Changes in causes of death in systemic sclerosis, 1972-2002. Ann Rheum Dis. 2007;66:940-4.

5. Benucci M, Bernardini P, Coccia C, et al. JAK inhibitors and autoimmune rheumatic diseases. Autoimmun Rev. 2023;22:103276.

6. Xin P, Xu X, Deng C, et al. The role of JAK/STAT signaling pathway and its inhibitors in diseases. Int Immunopharmacol. 2020;80:106210.

7. Raja J, Denton CP. Cytokines in the immunopathology of systemic sclerosis. Semin Immunopathol. 2015;37:543-57.

8. Wang W, Bhattacharyya S, Marangoni RG, et al. The JAK/STAT pathway is activated in systemic sclerosis and is effectively targeted by tofacitinib. J Scleroderma Relat Disord. 2020;5:40-50.

9. Lescoat A, Lelong M, Jeljeli M, et al. Combined anti-fibrotic and anti-inflammatory properties of JAK-inhibitors on macrophages *in vitro* and *in vivo*: perspectives for scleroderma-associated interstitial lung disease. Biochem Pharmacol. 2020;178:114103.

10. Bellamri N, Lelong M, Joannes A, et al. Effects of ruxolitinib on fibrosis in preclinical models of systemic sclerosis. Int Immunopharmacol. 2023;116:109723.

11. Karatas A, Oz B, Celik C, et al. Tofacitinib and metformin reduce the dermal thickness and fibrosis in mouse model of systemic sclerosis. Sci Rep. 2022;12:2553.

12. Dees C, Tomcik M, Palumbo-Zerr K, et al. JAK-2 as a novel mediator of the profibrotic effects of transforming growth factor β in systemic sclerosis. Arthritis Rheum. 2012;64:3006-15.

13. Aung WW, Wang C, Xibei J, et al. Immunomodulating role of the JAKs inhibitor tofacitinib in a mouse model of bleomycin-induced scleroderma. J Dermatol Sci. 2021;101:174-84.

14. Okiyama N, Furumoto Y, Villarroel VA, et al. Reversal of CD8 T-cell-mediated mucocutaneous graft-versus-host-like disease by the JAK inhibitor tofacitinib. J Invest Dermatol. 2014;134:992-1000.

15. Zeiser R, Burchert A, Lengerke C, et al. Ruxolitinib in corticosteroid-refractory graft-versus-host disease after allogeneic stem cell transplantation: a multicenter survey. Leukemia. 2015;29:2062-8.

16. Hurabielle C, Sicre de Fontbrune F, Moins-Teisserenc H, Coman T, et al. Efficacy and tolerance of ruxolitinib in refractory sclerodermatous chronic graft-versus-host disease. Br J Dermatol. 2017;177:e206-e8.

17. King B, Lee AI, Choi J. Treatment of hypereosinophilic syndrome with cutaneous involvement with the JAK inhibitors tofacitinib and ruxolitinib. J Invest Dermatol. 2017;137:951-4.

18. Scheinberg M, Sabbagh C, Ferreira S, et al. Full histological and clinical regression of morphea with tofacitinib. Clin Rheumatol. 2020;39:2827-8.

19. Tang JC, Zheng WY, Han GM, et al. Successful treatment of paediatric morphea with tofacitinib. Acta Derm Venereol. 2023;103:adv4805.

20. Karalilova RV, Batalov ZA, Sapundzhieva TL, Matucci-Cerinic M, Batalov AZ. Tofacitinib in the treatment of skin and musculoskeletal involvement in patients with systemic sclerosis, evaluated by ultrasound. Rheumatol Int. 2021;41:1743-53.

21. Khanna D, Padilla C, Tsoi LC, et al. Tofacitinib blocks IFN-regulated biomarker genes in skin fibroblasts and keratinocytes in a systemic sclerosis trial. JCI Insight. 2022;7:e159566.

22. You H, Xu D, Hou Y, et al. Tofacitinib as a possible treatment for skin thickening in diffuse cutaneous systemic sclerosis. Rheumatology. 2021;60:2472-7.

23. Komai T, Shoda H, Hanata N, et al. Tofacitinib rapidly ameliorated polyarthropathy in a patient with systemic sclerosis. Scand J Rheumatol. 2018;47:505-6.

Başıbüyük and Birlik. Janus Kinase Inhibitors in Systemic Sclerosis

Rheumatology Quarterly 2024;2(3):108-12

24. Moriana C, Moulinet T, Jaussaud R, et al. JAK inhibitors and systemic sclerosis: a systematic review of the literature. Autoimmun Rev. 2022;21:103168.

25. Winthrop KL, Cohen SB. Oral surveillance and JAK inhibitor safety: the theory of relativity. Nat Rev Rheumatol. 2022;18:301-4.

26. Balanescu AR, Citera G, Pascual-Ramos V, et al. Infections in patients with rheumatoid arthritis receiving tofacitinib versus tumour necrosis factor inhibitors: results from the open-label, randomised controlled ORAL Surveillance trial. Ann Rheum Dis. 2022;81:1491-503.

27. Benucci M, Damiani A, Infantino M, et al. Cardiovascular safety, cancer and Jak-inhibitors: dfferences to be highlighted. Pharmacol Res. 2022;183:106359.

EARLY AND LATE HISTOPATHOLOGICAL AND RADIOLOGICAL FINDINGS OF DIFFERENT ANIMAL SPECIES AND STRAINS IN A BLEOMYCIN-INDUCED ANIMAL MODEL

Duygu Temiz Karadağ[1], Seda Duman Öztürk[2], Özgür Çakır[3], Cüneyt Özer[4], Gürler Akpınar[5], Murat Kasap[5], Ayten Yazıcı[1], Ayşe Çefle[1]

[1]Kocaeli University Faculty of Medicine, Department of Internal Medicine, Division of Rheumatology, Kocaeli, Turkey
[2]Kocaeli University Faculty of Medicine, Department of Pathology, Kocaeli, Turkey
[3]Kocaeli University Faculty of Medicine, Department of Radiology, Kocaeli, Turkey
[4]Kocaeli University Experimental Medicine Research Unit (KOU DETAB), Kocaeli, Turkey
[5]Kocaeli University Faculty of Medicine, Department of Medical Biology, Kocaeli, Turkey

Abstract

Aim: Animal species and strains exhibit varying degrees of sensitivity to bleomycin-induced dermal fibrosis. This study aimed to establish early (week 2) and late (week 4) changes in bleomycin-induced skin fibrosis in two species (mice and rats) and three strains (BALB/C mice, C57BL/6 mice, Wistar rats) using histopathological and radiological analyses.

Material and Methods: Female C57BL/6 and BALB/C mice (n=4 each, 20-25 g, six weeks old) and female Wistar rats (n=4, 200-250 g, six weeks old) were subjected to subcutaneous bleomycin (10 mg/kg/day) or phosphate-buffered saline (PBS) every other day for four weeks. Skin biopsies from the four dorsal quadrants were analyzed for collagen homogenization, eosinophil and basophil counts, inflammatory response, and histological skin thickness (from 3 sections and ten different high-power fields in each biopsy).

Results: The collagen homogenization score, eosinophil density, mast cell density, inflammatory response score, and skin thickness were higher in the bleomycin group than in the PBS group across all models. Collagen scores were similar across models, but the inflammatory response and eosinophil and mast cell densities were higher at week 2 than at week 4. The highest inflammatory response scores at week 2 were observed in the BALB/C and Wistar mice. Histological skin thickness was greatest in Wistar rats at weeks 2 and 4.

Conclusion: The early inflammatory response was more severe in the BALB/C and Wistar models, although all models showed comparable collagen density and skin thickness. Wistar rats exhibited the most consistent parameters, making them suitable models for bleomycin-induced dermal fibrosis.

Keywords: Systemic sclerosis, animal model, mouse, rat, skin fibrosis

Address for Correspondence: Duygu Temiz Karadağ, Kocaeli University Faculty of Medicine, Department of Internal Medicine, Division of Rheumatology, Kocaeli, Turkey
Phone: +90 262 303 89 14 **E-mail:** dr_dtemiz@hotmail.com **ORCID ID:** orcid.org/0000-0002-5891-2032

Temiz Karadağ et al. Findings in Bleomycin-Induced Animal Models

Rheumatology Quarterly 2024;2(3):113-20

INTRODUCTION

Systemic sclerosis (SSc) is a complex autoimmune disorder characterized by excessive fibrosis, inflammation of the skin and internal organs, autoantibody positivity, and vascular damage (1). Fibrosis is the hallmark feature of SSc and is believed to stem from the activation and differentiation of fibroblasts into apoptosis-resistant myofibroblasts. The increased expression of myofibroblasts further catalyzes the formation of extracellular matrix (ECM), resulting in abnormal collagen deposition and pathological tissue remodeling (2). Despite considerable advancements, our understanding of the pathophysiology and key events driving persistent and uncontrolled fibroblast activation and ECM protein deposition remains incomplete (3). Consequently, there is an urgent need to elucidate the interplay between alterations in central targets to interrupt the damage cascade that precipitate disease onset. This strategy is critical for refining current therapeutic approaches for SSc, which remains one of the most devastating rheumatologic conditions to date (4).

Animal models that mimic one or more aspects of SSc have been established and are gaining recognition as valuable resources. They play a pivotal role in identifying the molecular mediators and signaling pathways involved in pathogenesis and conducting preclinical investigations to assess potential disease-modifying treatments (5,6).

Nonetheless, it is crucial to acknowledge that no single experimental model comprehensively mirrors the entire pathophysiological spectrum of human SSc. Despite their limitations, these models provide valuable insights into the mechanisms underlying unchecked fibrosis in SSc and other abnormalities associated with organ fibrosis (5,6).

The murine model of bleomycin-induced dermal fibrosis is widely used to investigate alterations occurring at various stages of the disease (7). First introduced by Yamamoto (8), the bleomycin-induced skin fibrosis model has been extensively utilized in both preclinical and pharmacological investigations. In addition to its local effects on the skin, high-dose subcutaneous bleomycin injections are believed to trigger a systemic autoimmune response characterized by the presence of autoantibodies, such as anti-nuclear autoantibodies, anti-Scl-70, and anti-U1 RNP, along with the induction of lung fibrosis. Studies have shown that bleomycin injection results in early inflammatory infiltrates comprising mononuclear cells in the skin, followed by the development of thickened dermal collagen bundles within approximately four weeks (9,10). Nonetheless, limited data are available on early and late changes in animal models generated using bleomycin across different species and strains.

Given the significance of the bleomycin-induced model of SSc in elucidating the pathogenesis of fibrotic skin changes, we investigated the early and late alterations of dermal fibrosis in the skin of two animal species, including two widely utilized mouse strains. Our hypothesis was that different species and strains manifest varying degrees of sensitivity to bleomycin-induced dermal fibrosis. The primary aim of this study was to establish methods for inducing a standardized model of fibrosis in adult rat and mouse skin. The insights gained from this investigation can serve as a reference for selecting an appropriate animal model that demonstrates morphological and histological consistency with both the early and late stages of SSc-associated skin fibrosis.

MATERIALS AND METHODS

Animals

C57BL/6 (n=4) and BALB/C (n=4) female mice weighing 20-25 g at 6-8 weeks of age and Wistar female rats weighing 200-250 g (n=4) were utilized in the study. In this study, we chose female animals to minimize the variability associated with hormonal changes that may occur in males. Literature shows that fibrosis severity can differ between sexes, and our selection aims to reduce additional sources of experimental variability. Animals were randomized into two equal groups: (I) phosphate-buffered saline (PBS)-injected and (II) bleomycin-treated groups (Figure 1). Due to known variations in bleomycin activity between batches, a unit/mL regime is generally recommended over a mg/mL regime to ensure consistent bleomycin activity. In our study, a mg/mL formulation was used, but all dosage calculations were carefully adjusted based on individual animal body weight. When changing variables such as species, age, or sex, it is important to optimize the dosage accordingly to maintain experimental reproducibility. For the early-stage SSc model, half of the animals were sacrificed at the end of the second week. The remaining animals in both groups completed the 4-week period for the late-stage SSc model. PBS and bleomycin were administered subcutaneously on weekdays (5 days) and every other day. No injections were administered on weekends (2 days). The injections were administered on the dorsal median line 1 cm superior to the tail base and 0.5 cm lateral to the right. Bleomycin (15 mg) was diluted in 15 mL of saline (1 mg/mL) and administered at a dose of 10 mg/kg (e.g., 2 mL for a 200 g rat). Similar dosages were administered to the PBS group, with 0.01 mL of PBS injected per kg. at the end of the second week, animals in the early disease arms (PBS and Bleomycin) were euthanized (n=16). The assumption that skin changes at week 2 reflect the early stage of SSc was based on previous studies (8). The dorsal region of
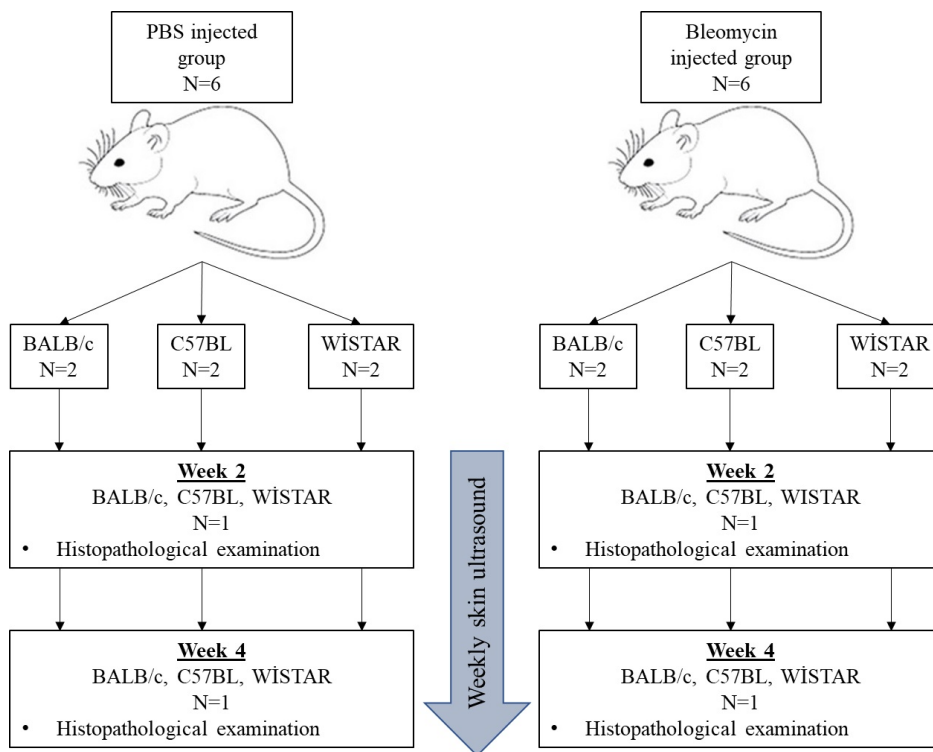
Figure 1. Schematic illustrating the procedures to be performed on the rats in the animal model
PBS: Phosphate-buffered saline

the euthanized animals was divided into four quadrants, and full-thickness skin biopsies (1x1 cm) were obtained from each quadrant for histopathological examination. The tissue samples were placed in formaldehyde for histopathological analysis. For the late-stage disease model, animals not euthanized continued to receive PBS or bleomycin injections. At the end of week 4, all animals in the late-stage disease model were euthanized. The dorsal region of euthanized animals was similarly divided into four quadrants, and full-thickness skin biopsies (1x1 cm) were obtained from each quadrant (Figure 2).

The study was approved by the Kocaeli University Animal Research Ethics Committee (approval number: KOU. Haydek2023/1, date: 31.01.2024).

Ultrasonography

High-frequency ultrasound was used to measure skin thickness weekly to assess skin thickening. This allowed us to evaluate whether the procedure-induced skin thickening and to compare skin thickness measurements between ultrasound and histopathological examination. Prior to ultrasound imaging, excess hair on the mice skin was gently shaved to prevent interference. Skin thickness was measured using ultrasound from the dorsal region of the animals (1 cm to the right and left
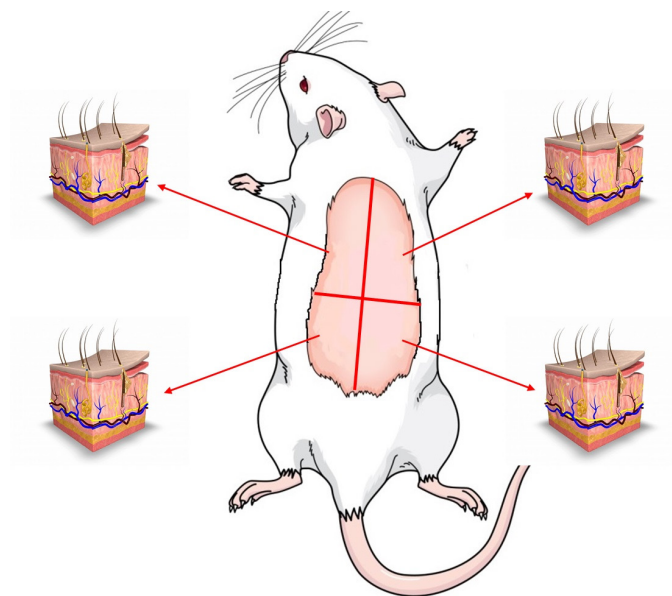

Figure 2. Schematic representation of the areas in the dorsal region of the experimental animal from which skin tissue samples will be collected

of the vertebrae, respectively) twice for each animal. Ultrasound measurements were performed longitudinally on the vertebrae using a linear probe (4-20 MHz, Esaote MyLab X9, Italy), and images were recorded (Figure 3). In the images, the epidermis-dermis thickness was manually determined by drawing a straight line, and measurements were taken from three different locations in each image, with the average being calculated.

Histopathological Examination

The collected tissues were fixed in formaldehyde for histopathological examination. Sections of skin tissue embedded in paraffin were obtained at a thickness of 4 m. The sections were stained with hematoxylin and eosin (H&E) and examined under a light microscope. Immunohistochemical staining of tissue sections was performed according to the manufacturer's protocol. Histopathological examination was performed to evaluate skin thickness, inflammation, and fibrosis. Histological skin thickness was determined by manually drawing a straight line from the epidermis surface to subdermal adipose tissue. Skin thickness was evaluated by measuring four different sections of each biopsy sample and three different areas within each section. The results were reported as the average of the measurements. Inflammation was assessed based on the density of inflammatory cells. The number of inflammatory cells was calculated from H&E sections. The total inflammation score was based on the inflammatory response score, which was calculated using the total number of inflammatory cells in the sections. The inflammatory response score was determined by measuring four sections and three times within each section from four regions in the high-power field (x40 magnification) of each biopsy sample. The inflammatory response score was scored between 0 and 2

based on the density of all inflammatory cells (0-2=0; 3-7=1; ≥8=2). The numbers of eosinophils and basophils were similarly evaluated in four sections and

three times within each section from four regions in the high-power field (x40 magnification) of each biopsy sample from H&E sections. The degree of fibrosis density was scored from 0 to 3 based on the thickness and tightness of the collagen fibers, and the collagen homogenization score was calculated. The evaluation was performed by measuring from four sections and three times within each section from four regions in the high-power field (x40 magnification) of each biopsy sample.

RESULTS

Histopathological examination results are presented in Table 1. Collagen homogenization scores were higher in the bleomycin group than in the PBS group in both early and late stages (2 and 4 weeks) in all animals (BALB/C, C57BL/6, Wistar) (2 weeks: 1.75±0.5 vs. 0; 2 vs. 0.25±0.5; 2 vs. 0; 4 weeks: 1.75±0.5 vs. 0.5±0.58; 2 vs. 0.25±0.5; 2 vs. 0).

However, no difference was observed in collagen homogenization scores between the early and late stages of bleomycin treatment in animals.

Histological skin thickness was higher in the bleomycin-treated group than in the PBS group in all animals in the early stage (2 weeks) (1.68±0.47 vs. 0.04±0.054; 1.73±0.46 vs. 0.023±0.022; 2.25±0.51 vs. 0.068±0.066, respectively). In the late stage (4 weeks), higher histological skin thickness was observed in the bleomycin arm than in the PBS arm in C57BL/6 and Wistar strains (1.2±0.36 vs. 0.016±0.019; 3.28±0.36 vs. 0.028±0.017, respectively). Only Wistar rats reached the highest skin thickness
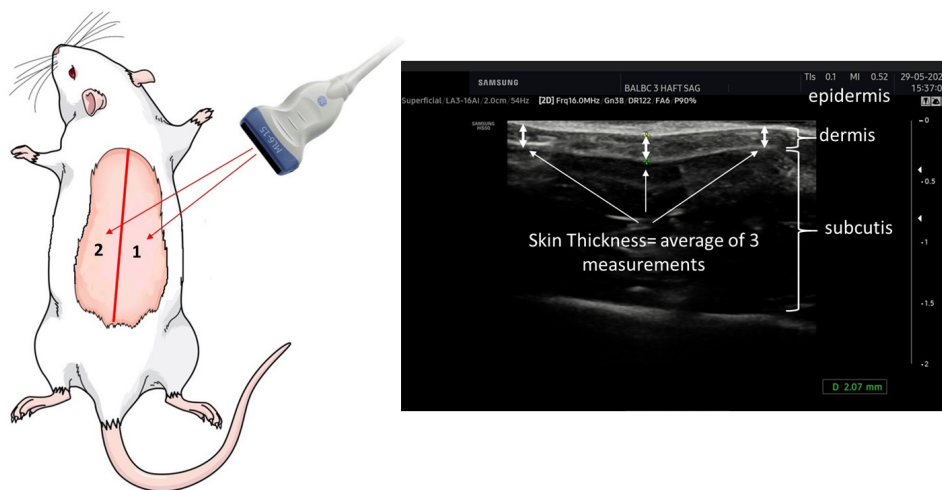

Figure 3. Schematic representation of skin measurement using ultrasound conducted in our pilot study. Along with an ultrasound image showing the measured skin tissue in a rat

at week 4 when comparing early- and late-stage histological skin thickness in animals administered bleomycin (3.28±0.36 vs. 2.25±0.51) (Figure 4).

Inflammation, as measured by eosinophil and basophil counts and the inflammatory response score, was higher in the bleomycin group than in the PBS group in all animals at the early stage (Table 1). In the early stage (2 weeks), compared with the late stage (4 weeks), the bleomycin group showed higher eosinophil count (8.25±1.71 vs. 2.5±1.73; 3±2.58 vs. 0; 7±1.41 vs. 0), basophil count (9.75±2.76 vs. 1.25±0.96; 4.25±3.30 vs. 0; 9.5±1.29 vs. 0), and inflammatory response score (1.75±0.5 vs. 0.75±0.5; 0.75±0.5 vs. 0; 1.5±0.58 vs. 0).

Table 1. Variation in histopathological changes between the drug (BLM) and control (PBS) arms at weeks 2 and 4 based on animal species and strains

	Collagen homogenization score		Eosinophil count		Basophil count		Inflammatory response score		Histological skin thickness	
	Week 2	Week 4	Week 2	Week 4	Week 2	Week 4	Week 2	Week 4	Week 2	Week 4
BALB/C										
BLM (n=1)	1.75±0.5	1.75±0.5	8.25±1.71	2.5±1.73	9.75±2.76	1.25±0.96	1.75±0.5	0.75±0.5	1.68±0.47	1.21±1.42
PBS (n=1)	0	0.5±0.58	1.25±2.5	0	1.25±2.5	0	0.25±0.5	0	0.04±0.054	1.29±0.69
C57BL/6										
BLM (n=1)	2	2	3±2.58	0	4.25±3.30	0	0.75±0.5	0	1.73±0.46	1.2±0.36
PBS (n=1)	0.25±0.5	0.25±0.5	0.5±1	0	1±2	0	0.25±0.5	0	0.023±0.022	0.016±0.019
Wistar										
BLM (n=1)	2	2	7±1.41	0	9.5±1.29	0	1.5±0.58	0	2.25±0.51	3.28±0.36
PBS (n=1)	0	0	2.5±2.38	0	0	0	0.75±0.5	0	0.068±0.066	0.028±0.017
PBS: Phosphate-buffered saline, BLM: Bleomycin										

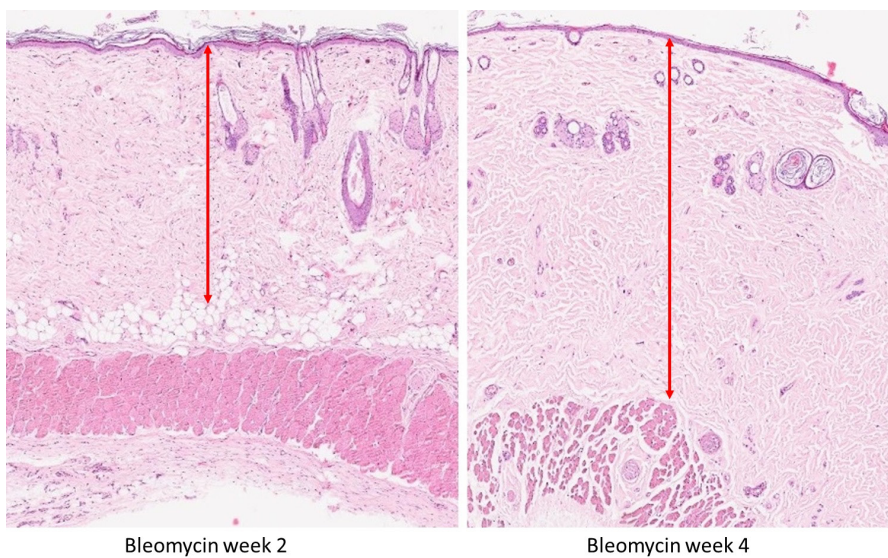Bleomycin week 2   Bleomycin week 4

Figure 4. Differential collagen levels in the skin fibrosis tissue induced by bleomycin were observed in the early (2nd week) and late (4th week) stages in Wistar (during the 4 week of bleomycin application, an increase in skin thickness and tightening of collagen fibrils)

Temiz Karadağ et al. Findings in Bleomycin-Induced Animal Models

Rheumatology Quarterly 2024;2(3):113-20

Ultrasonographic measurements of skin thickness revealed higher measurements in animals treated with bleomycin than in those in the PBS group during the first weeks. From the last week onwards, skin thickness has decreased and approached that of the PBS group, except for Wistar rats. Bleomycin application significantly increased skin thickness at two weeks, followed by a decrease in the rate of skin thickness increase, reaching a plateau at week 3, and then decreasing from week four onwards (Figure 5).

DISCUSSION

Numerous murine and avian models are available to explore diverse aspects of SSc, including vasculopathy, inflammation, autoimmunity, and fibrosis. However, none of these models fully recapitulates all features of human SSc. Therefore, a rigorous selection of animal models is essential for successful *in vivo* studies. Bleomycin-induced dermal fibrosis has been established in various mouse strains, although symptom severity and the time required to induce dermal sclerosis. In this study, we aimed to investigate the changes in bleomycin-induced skin fibrosis in two different species (mice and rats) and three different animal strains (BALB/C mice, C57BL/6 mice, and Wistar rats). Additionally, we examined the differences in inflammatory and fibrotic characteristics occurring in the early (2 weeks) and late (4 weeks) stages of our model, both within each model and across the different animal models.

The bleomycin-induced skin fibrosis model offers a straightforward establishment process that can be applied to various mouse strains. This tool serves as a valuable tool for evaluating anti-inflammatory and antifibrotic therapies in preclinical studies of SSc. This model boasts advantages such as ease of implementation, widespread accessibility, and

reproducibility, fulfilling essential criteria for a reliable animal model (10). The initial surge in proinflammatory cytokines [interleukin-1 (IL-1), tumor necrosis factor-alpha, IL-6, interferon-gamma] is succeeded by heightened expression of growth factors (transforming growth factor-beta 1) and extracellular components, peaking around day 14. The transition from inflammation to fibrosis typically occurs around day 9 following the initiation of bleomycin exposure. Sclerotic changes induced by bleomycin persist for at least six weeks following cessation of bleomycin injections (11,12). According to our results, compared with the control group (PBS) across all three models, we noted a substantial increase in both collagen content (collagen homogenization score) and inflammation (eosinophil count, basophil count, and inflammatory response score) at both weeks. Our findings indicated a higher level of inflammation in the BALB/C mouse model. Interestingly, we observed similar collagen homogenization scores in the early and late stages of each animal model. We interpreted this observation as potentially stemming from an increase in collagen fiber density and alterations in the molecular structure over time due to ongoing injections without resulting in discernible differences in semi-quantitative assessments.

One of the outcomes of our study revealed a notable increase in histological skin thickness compared with the control group (PBS) across all animal models during the early stage (2 weeks). However, histological skin thickness during the late stage (4 weeks) exhibited variation, with the application of bleomycin failing to induce a similar increase in the second late stage as observed in the early stage for all animals. To minimize animal sacrifice, we refrained from evaluating histological skin thickness measurements at weeks 1 and 3. Instead, we compared the radiological skin thickness measurements obtained through
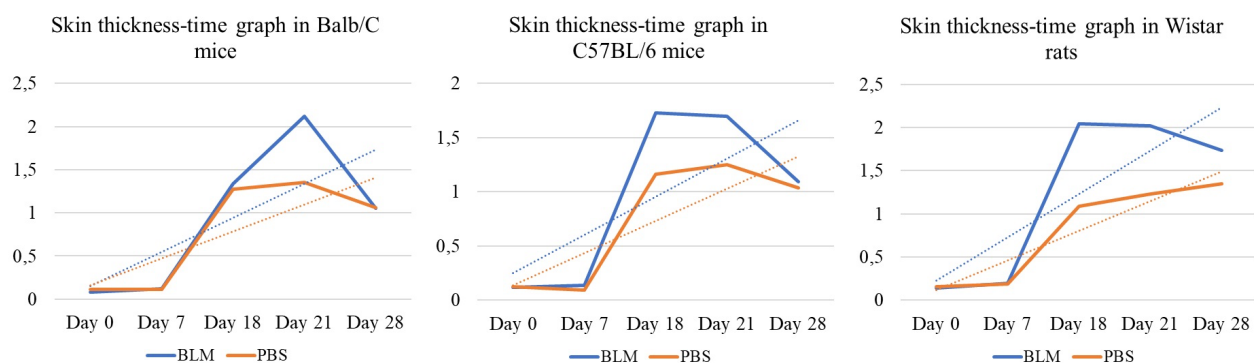

Figure 5. Variation in skin thickness over time among different animals using high-frequency ultrasound
PBS: Phosphate-buffered saline, BLM: Bleomycin

Rheumatology Quarterly 2024;2(3):113-20

Temiz Karadağ et al. Findings in Bleomycin-Induced Animal Models

weekly high-frequency ultrasound assessments with the histological measurements. The radiological skin thickness measurements supported the observed increase in histological skin thickness, reaching a peak level at week 2, followed by a decrease in the rate of increase at week 3 and a subsequent decrease in skin thickness in all animals receiving bleomycin by week 4. The ultrasound results corroborated our histopathological findings. Histologically, we observed the thickest skin in Wistar rats during both the early and late stages. We interpreted this finding as suggestive of ongoing bleomycin application in the late stages, potentially leading to changes in collagen structure rather than only an increase in skin thickness and collagen content, which is consistent with the interpretation for collagen homogenization scores.

The number of studies that concurrently compared different species and strains in the literature is limited. In a study by Ruzehaji et al. (13), a group of male BALB/C (n=6), C57BL/6 (n=6), and DBA/2 (n=6) mice were subjected to bleomycin every other day for 21 days to investigate whether sex and mouse strain influence the severity of dermal fibrosis.

They observed the successful induction of dermal fibrosis by bleomycin in all three assessed strains, with the highest severity observed in BALB/C mice regardless of sex. Notably, female BALB/C mice exhibited greater susceptibility to bleomycin-induced dermal fibrosis compared with their female counterparts in the C57BL/6 and DBA/2 strains. Regarding dermal thickness, hydroxyproline levels, and myofibroblast counts, no significant differences were noted between male and female BALB/C and C57BL/6 mice. Male DBA/2 mice had a higher number of myofibroblasts than female DBA/2 mice. Furthermore, the inflammatory cell counts were significantly lower in male DBA/2 mice treated with bleomycin than in male BALB/C and C57BL/6 mice treated with the same. Interestingly, dermal thickness did not differ between mice administered daily bleomycin injections and those administered injections every other day.

However, compared with daily bleomycin injections, bleomycin injections administered every other day increased basal hydroxyproline levels, a biochemical marker of collagen. Moreover, there were no discernible differences in dermal thickness, hydroxyproline content, or myofibroblast counts between mice injected with bleomycin at concentrations of 0.5 mg/mL compared to those injected with 1 mg/mL bleomycin (13).

One of the most significant limitations of our study is the small number of animals. Due to the use of multiple species and strains in our study, a large number of animals was avoided. To minimize the bias resulting from this limitation, we maintained a high number of tissue samples taken from each animal and examined a high number of sections from each tissue sample. Another limitation was the use of H&E staining instead of immunohistochemical staining to identify inflammatory cells. Despite these limitations, one of the strengths of our study was that, in addition to histological examination, we simultaneously assessed the increase in skin thickness radiologically using high-frequency ultrasound.

CONCLUSION

In this study, we investigated the influence of genetic background on the induction of experimental dermal fibrosis. Our findings suggest that bleomycin injection induces dermal fibrosis in BALB/C and C57BL/6 mice as well as Wistar rats. Notably, inflammation was prominently observed in the early phase of the model and was characterized by the highest skin thickness. Increased collagen content persisted in the late phase despite a decrease in skin thickness at this stage.

Although BALB/C mice exhibit a higher level of inflammatory response than other models, Wistar rats met all the criteria for the model. These observations underscore the importance of selecting an appropriate protocol for inducing dermal fibrosis, which is relevant for pharmacological testing and therapeutic interventions. Although numerous studies in the literature have utilized animal models induced with bleomycin, concurrent assessments of different species and strains are needed. Therefore, despite the limitations of our study, our findings contribute to addressing these gaps in the literature and improve our understanding of this issue.

Temiz Karadağ et al. Findings in Bleomycin-Induced Animal Models

Rheumatology Quarterly 2024;2(3):113-20

REFERENCES

1.   Allanore Y, Simms R, Distler O, et al. Systemic sclerosis. Nat Rev Dis Primers. 2015;1:15002.

2.   Cutolo M, Soldano S, Smith V. Pathophysiology of systemic sclerosis: current understanding and new insights. Expert Rev Clin Immunol. 2019;15:753-64.

3.   Van Caam A, Vonk M, Van Den Hoogen F, Van Lent P, Van Der Kraan P. Unraveling SSc pathophysiology; the myofibroblast. Front Immunol. 2018.

4.   Giacomelli R, Liakouli V, Berardicurti O, et al. Interstitial lung disease in systemic sclerosis: current and future treatment. Rheumatol Int. 2017;37:853-63.

5.   Asano Y, Sato S. Animal models of scleroderma: current state and recent development. Curr Rheumatol Rep. 2013;15:382.

6.   Tsujino K, Sheppard D. Critical appraisal of the utility and limitations of animal models of scleroderma. Curr Rheumatol Rep. 2016;18:4.

7.   Marangoni RG, Varga J, Tourtellotte WG. Animal models of scleroderma: recent progress. Curr Opin Rheumatol. 2016;28:561-70.

8.   T Yamamoto. Animal model of systemic sclerosis. J Dermatol. 2010;37:26-41.

9.   Bi X, Mills T, Wu M. Animal models in systemic sclerosis: an update. Curr Opin Rheumatol. 2023;35:364-70.

10. Yamamoto T, Takagawa S, Katayama I, et al. Animal model of sclerotic skin. I: Local injections of bleomycin induce sclerotic skin mimicking scleroderma. J Invest Dermatol. 1999;112:456-62.

11. Yoshizaki A, Iwata Y, Komura K, et al. CD19 regulates skin and lung fibrosis via Toll-like receptor signaling in a model of bleomycin-induced scleroderma. Am J Pathol. 2008;172:1650-63.

12. Takagawa S, Lakos G, Mori Y, Yamamoto T, Nishioka K, Varga J. Sustained activation of fibroblast transforming growth factor-beta/Smad signaling in a murine model of scleroderma. J Invest Dermatol. 2003;121:41-50.

13. Ruzehaji N, Avouac J, Elhai M, et al. Combined effect of genetic background and gender in a mouse model of bleomycin-induced skin fibrosis. Arthritis Res Ther. 2015;17:145.

USING ENSEMBLE LEARNING AND FEATURE SELECTION IN THE DIAGNOSIS OF LOW BACK PAIN

Yüksel Maraş[1], Ahmet Kor[2], Semra Duran[3], Kevser Orhan[4], Ebru Atalar[4], Emine Sena Sözen[4], Kemal Üreten[5], Hadi Hakan Maraş[6]

[1]University of Health Sciences Turkey, Ankara Bilkent City Hospital, Clinic of Rheumatology, Ankara, Turkey
[2]Aksaray Training and Research Hospital, Clinic of Rheumatology, Aksaray, Turkey
[3]University of Health Sciences Turkey, Ankara Bilkent City Hospital, Clinic of Radiology, Ankara, Turkey
[4]University of Health Sciences Turkey, Ankara Bilkent City Hospital, Clinic of Rheumatology, Ankara, Turkey
[5]Çankaya University Faculty of Engineering, Department of Computer Engineering, Ankara, Turkey
[6]Çankaya University Vocational School, Department of Computer Programming, Ankara, Turkey

Abstract

Aim: A wide variety of research is currently being conducted on how artificial intelligence can assist clinical decision-making and improve clinician judgments. The goal of this research was to develop a computer-aided diagnostic (CAD) approach that can aid healthcare professionals in identifying lumbosacral pathologies.

Material and Methods: The study included 633 abnormal and 442 normal lateral lumbosacral radiographs, and the You Only Look Once algorithm was used to automate the cropping task. This study used pre-trained VGG-16, ResNet-101, and MobileNetV2 models for transfer learning. Feature extraction was performed from the intermediate layer of VGG-16, resulting in 512 features. Then, a variance threshold was applied, resulting in 221 selected features with a variance threshold of 0.01. Then, support vector classifier, logistic regression, random forest classifier, and k-nearest neighbours machine learning models were trained using both sets of 512 extracted features and 221 selected features separately.

Results: The results from the ensemble learning model with the stacking classifier using features selected using a threshold value 0.01 from features extracted were: accuracy 93.0% (best); sensitivity, 91.8%; specificity, 94.1%; precision, 92.9%; F1 score, 92.3% (best); area under the receiver operating characteristic curve, 0.97 (one of the best); and Cohen's kappa, 0.86 (best).

Conclusion: The ensemble learning model with a stacking classifier using features selected by using a threshold value of 0.01 from features extracted by processing the intermediate layer of VGG-16 performs better than the transfer learning models using pre-trained networks, such as VGG-16, ResNet-50, and MobileNetV2, and the learning methods that do not apply feature selection in distinguishing lumbar vertebral pathologies.

Keywords: Artificial intelligence, computer-aided diagnosis, convolutional neural networks, deep learning, low back pain, machine learning, ensemble learning, feature selection

Address for Correspondence: Yüksel Maraş, University of Health Sciences Turkey, Ankara Bilkent City Hospital, Clinic of Rheumatology, Ankara, Turkey
Phone: +90 555 332 97 40 **E-mail:** ymaras@hotmail.com **ORCID ID:** orcid.org/0000-0001-9319-0955

Maraş et al. Computerized Diagnosis of Low Back Pain

Rheumatology Quarterly 2024;2(3):121-9

INTRODUCTION

Chronic low back pain (lumbar spine pain) is a widespread problem that most people experience at some point in their lives (1). It is rarely fatal, and it is usually benign and self-limiting. The first step in managing lumbar low back pain is plain radiography, which often provides an anteroposterior and lateral view of the lumbar vertebrae (2). The most common causes of low back pain on plain radiography include disc space narrowing, osteophytes, spondylosis, endplate sclerosis, spondylolisthesis, and facet joint osteoarthritis (3).

The prevalence of low back pain is increasing and can result in decreased physical function. Plain radiographs are widely used in clinical practice because they are relatively inexpensive, are easy to apply, and have become standard for patients with low back pain (1,3).

The ordering clinician primarily evaluates plain radiographs of the lumbar spine. For this reason, computer-assisted diagnosis as a primary aid is becoming more common (4). Studies have shown that the success of diagnosis by clinicians can be increased through the use of a deep learning method (5-9).

Deep learning methods, a subset of machine learning, are effective in extracting complex features from raw data such as images, text, and audio. Convolutional neural networks (CNNs), which use a deep learning architecture, consist of many layers and have succeeded in image processing to retrieve information from images. Different CNN architectures have been developed for different purposes, such as classification, segmentation, object detection, and localization (10,11). Due to these features, deep learning methods have been successfully used in applications such as object recognition, speech recognition, face recognition, text analysis, language modeling, translation, autonomous vehicles, robotic applications, e-commerce, medical image analysis, disease diagnosis, and treatment planning. However, large amounts of data are required to implement CNNs for image classification, and it is difficult to find sufficient data in the medical field. Networks pre-trained on the Imagenet dataset consisting of natural images were successfully used to classify medical images using the transfer learning method (12-15). These pre-trained networks included AlexNet (16), GoogLeNet (17), VGG (18), ResNet (10), MobileNet (19), and DenseNet (20).

The region-based CNN (RCNN), Fast RCNN, Faster RCNN, and YOLO CNN architectures are used for segmentation and object detection (21,22). YOLO is fast and has been successfully applied to object detection tasks. It treats object detection as a regression problem and performs real-time object detection (45 frames per second) using a single CNN called DarkNet. The proposed YOLO model makes predictions for various bounding boxes of different sizes and aspect ratios to detect objects of diverse shapes and sizes. The non-max suppression algorithm selects the best option from the multiple projected bounding boxes (23). YOLO works with low-resolution images, and the algorithm is not very successful in detecting small objects; thus, other CNN structures are preferred for classification tasks.

Feature selection is the process of selecting informative and relevant features from a more extensive dataset that better characterizes multiple class patterns (24). Variance thresholding is a simple yet effective feature selection method that helps exclude low-variance features, reduce noise, and optimize input data.

The aim of this study was to develop a computer-aided diagnosis (CAD) method to assist clinicians in diagnosing lumbosacral pathologies. Plain lumbosacral radiography is primarily used for low back pain. Plain radiography is an easily accessible, inexpensive, and low-radiation method. Physicians may not have sufficient experience to evaluate plain lumbosacral radiographs, and some findings may be overlooked for reasons such as workload or carelessness. Clinicians can receive objective assistance in evaluating plain lumbosacral radiographs from the proposed CAD model.

MATERIAL AND METHODS

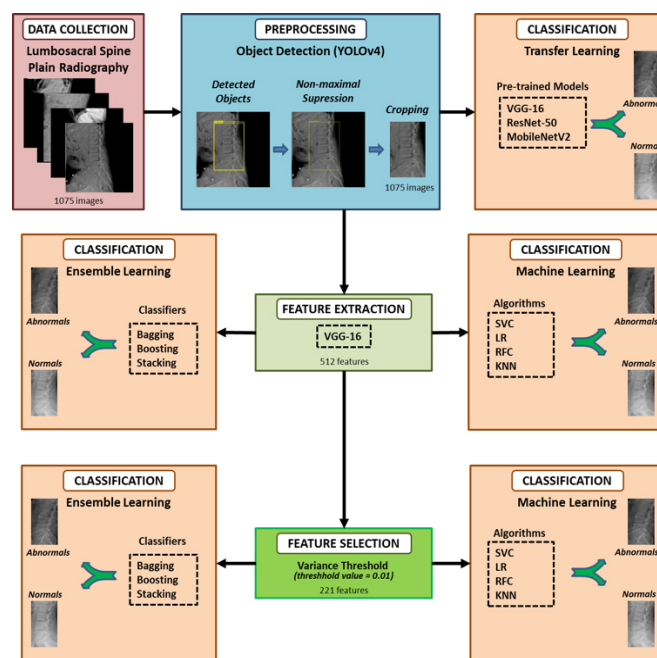An overview of the research architecture is presented in Figure 1.

Figure 1. Overview of proposed CNN research architecture
CNN: Convolutional neural network

Dataset

A dataset of images was obtained from plain lumbosacral radiographs of patients examined between January 1, 2020, and March 1, 2022 at the rheumatology outpatient clinic of University of Health Sciences Turkey, Ankara Bilkent City Hospital. Approval with a waiver of informed consent, including written permission from the radiology department, was obtained from the University of Health Sciences Turkey, Ankara Bilkent City Hospital Clinical Research Ethics Committee for the study (date: 09/03/2022, number: E1-22-2546). Radiographs with low image quality (a total of 122) were excluded before obtaining the final dataset, which contained 633 abnormal and 442 normal lateral lumbosacral radiographs. The lumbosacral radiographs were labeled independently by one rheumatology specialist and one radiology specialist with more than 10 years of experience. These authors did not include radiographs that were not labeled as belonging to the same class in the study.

Data Pre-processing

The radiographic images used in this study varied in dimensions, ranging from 300x2020 to 800x2020 pixels. In plain lumbosacral radiographs, various artifacts, such as patient name, date, number, and direction, could adversely affect training. The first lumbar vertebra and sacrum had to be cropped from the entire image to discard noisy areas that were unnecessary for training and to shorten the training period. The dataset contained 1075 images, and manually cropping these images would have been a labor-intensive and time-consuming task. The YOLO algorithm was used to automate the cropping process. A total of 30 images (24 for training and six for validation) were labeled in YOLO format by the rheumatologist. In addition, the YOLOv4 configuration file was adjusted to accommodate a single class. The YOLOv4 training parameters were configured with the following settings: batch size of 16, 8 subdivisions, momentum of 0.9, and learning rate of 0.001. The pre-trained Darknet53 YOLOv4 weights were utilized to retrain the network. After 2,000 iterations, the Keras TensorFlow environment was used to create an object detector with the obtained weights. A non-maximal suppression algorithm was employed to crop the bounding box regions automatically from all dataset images. The database stored the edited images, which were then classified. Two images of a patient's radiograph are displayed in Figure 2: (a) bounding boxes and (b) the final clipping rectangle determined after applying the non-maximum suppression algorithm. The image dataset was divided randomly into training (70%), validation (15%), and test sets (15%). The image distribution is presented in Table 1.

The hyperparameter tuning process utilized the validation dataset, and the model accuracy was assessed using the test set. The stochastic gradient descent with momentum technique was used for the optimization process. The other hyperparameters
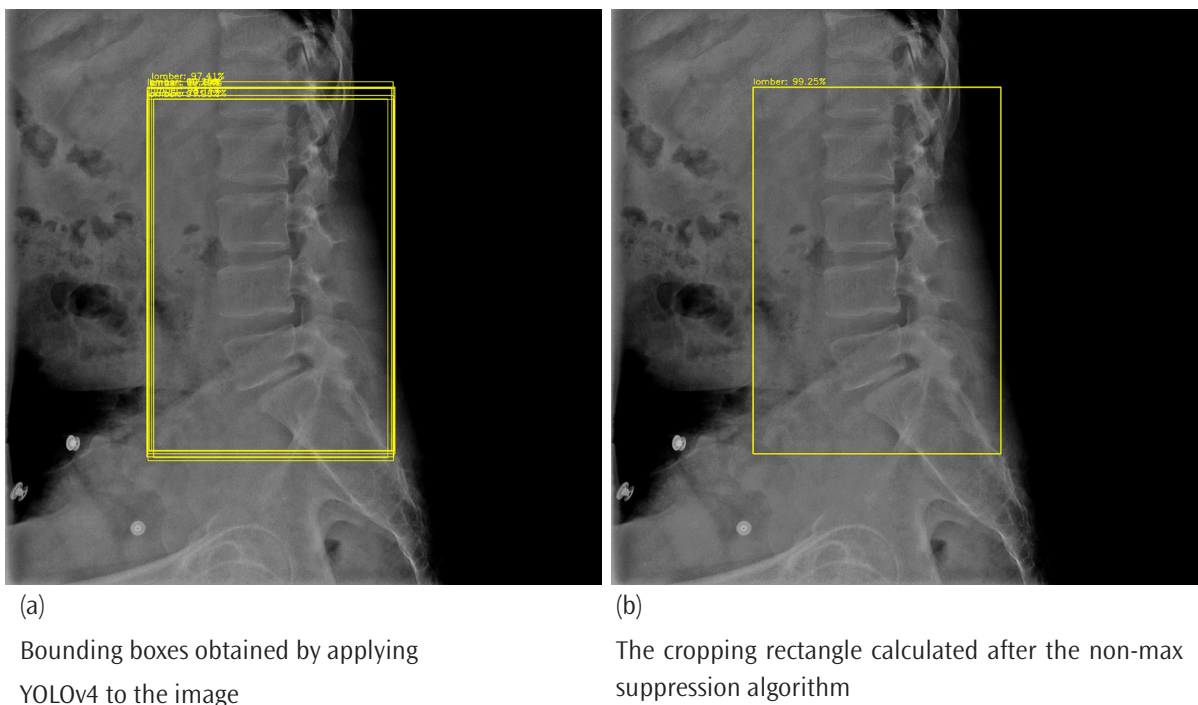

(a)

Bounding boxes obtained by applying YOLOv4 to the image

(b)

The cropping rectangle calculated after the non-max suppression algorithm

Figure 2. Outputs of feature selection process
YOLO: You Only Look Once

Maraş et al. Computerized Diagnosis of Low Back Pain

Rheumatology Quarterly 2024;2(3):121-9

for the experiments are set as follows: epoch is 25, the validation frequency is 16, mini batch size =16, the L2 regularization is set to 0.004, and initial learning rates =0.0003.

In our study, the variance thresholding method was applied to enhance the interpretability and efficiency of our CAD model, ensuring that selected features were meaningful for accurate diagnosis of lumbosacral pathology.

Data Processing Environment

The research was conducted using a computer with an Intel® Core™ i7-9750H CPU @ 2.60 GHz processor, an NVIDIA GeForce RTX 2060 graphics card, and 32 GB RAM, and it was operated on a 64-bit Windows 10 system. Python 3.9 was the programing language utilized within the Keras TensorFlow environment. Essential libraries were imported, and statistical calculations were performed using the Scikit-learn library.

Transfer Learning, Data Augmentation

Pre-trained models with varying characteristics, which were trained using natural images from the ImageNet dataset, were suitable for transfer learning. This study used pre-trained VGG-16, ResNet-50, and MobileNetV2 models for transfer learning.

Data augmentation can be applied when insufficient data are available. For the purpose of augmentation, we added slightly modified versions of the existing data to the dataset to enhance the model's accuracy and avoid overfitting. Rotation, translation, and flipping transformations were used for the images in this study for augmentation.

Statistical Analysis

Each model's performance was assessed using metrics such as accuracy, sensitivity, specificity, precision, F1 score, area under the receiver operating characteristic (ROC) curve (AUC), and Cohen's kappa coefficient. The confusion matrix and ROC curve were used to calculate these metrics. The deep learning toolbox was used to test the models and obtain a confusion matrix (TP:

True positive; FP: False positive; TN: True negative; FN: False negative).

RESULTS

The transfer learning method utilized pre-trained VGG-16, ResNet-50, and MobileNetV2 models. The models were tested on the test dataset after training. The accuracy, sensitivity, specificity, precision, F1 score, AUC, and Cohen's kappa coefficient values obtained for the VGG-16, ResNet-50, and MobileNetV2 models are presented in Table 2. The confusion matrix and ROC curve resulting from testing the VGG-16 model are depicted in Figure 3. Figure 4 shows the prediction results for four randomly selected images during testing with the VGG-16 model. A technique called gradient-weighted class activation mapping (Grad-CAM) was used to generate heatmaps that highlight important decision-making regions in the model (25,26). Figure 5 shows a lumbosacral plain radiography image obtained with Grad-CAM, indicating the regions that were important for model prediction.

Feature extraction was performed from the intermediate layer of VGG-16, resulting in 512 features. A variance threshold was then applied, resulting in 404 selected features with a variance threshold of zero and 221 selected features with a variance threshold of 0.01. Subsequently, ensemble learning models (Bagging, Boosting, and Stacking), and machine learning models [support vector classifier, logistic regression (LR), random forest classifier, and k-nearest neighbours (KNN)] were trained using both sets of all 512 extracted features and these 221 selected features separately. The ensemble model hyperparameters are shown in Table 3, the performance metrics are given in Tables 4-6 are for machine learning. Figure 6 shows the performance scores of the ensemble learning models before and after feature selection, and Figure 7 shows the performance scores of the machine learning. The suffix "b" denotes the scores prior to feature selection, and "a" represents the scores after feature selection.

Table 1. Numbers of images used for training, validation, and testing

	Training	Validation	Test	Total
Abnormal	458	80	95	633
Normal	319	56	67	442

Table 2. Performance metrics of VGG-16, ResNet-50, and MobileNetV2 pretrained models

Model	Accuracy (%)	Sensitivity (%)	Specificity (%)	Precision (%)	F1 score (%)	AUC	Kappa
VGG-16	89.5	92.5	87.3	83.7	87.9	0.95	0.78
ResNet-50	84.5	88.0	82.1	77.6	82.5	0.92	0.68
MobileNetV2	80.8	85.0	77.8	73.0	78.6	0.84	0.61
AUC: Area under the curve							

The overall performance of each model can be interpreted using the radar chart shown in Figure 8. Considering the assumptions "shape's size can reveal the model's power" and "the bigger the shape, the higher the performance", the ensemble learning method using the stacking classifier utilizing only the selected features can be the most robust model.
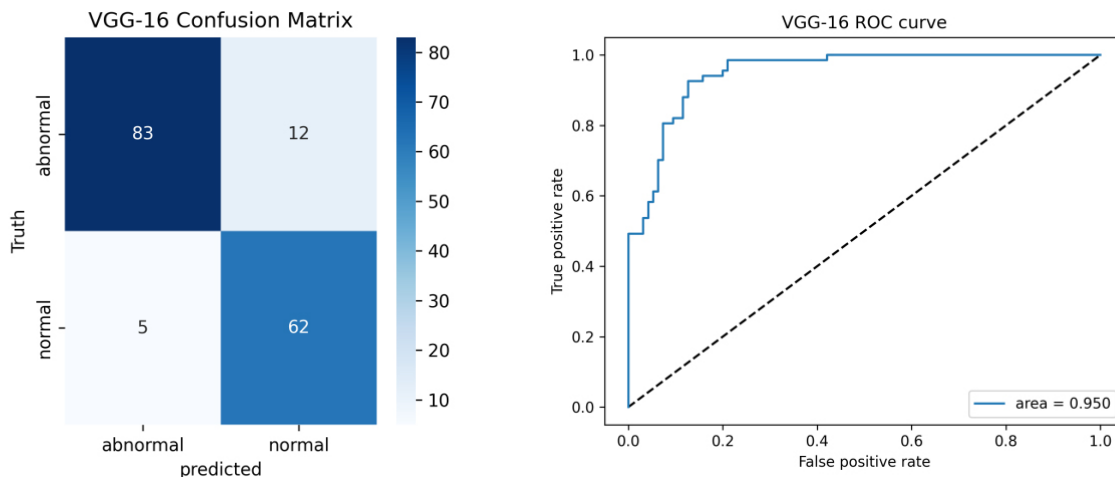
Figure 3. Confusion matrix (left) and receiver operating characteristic curve (right) obtained during testing of the VGG-16 model
ROC: Receiver operating characteristic
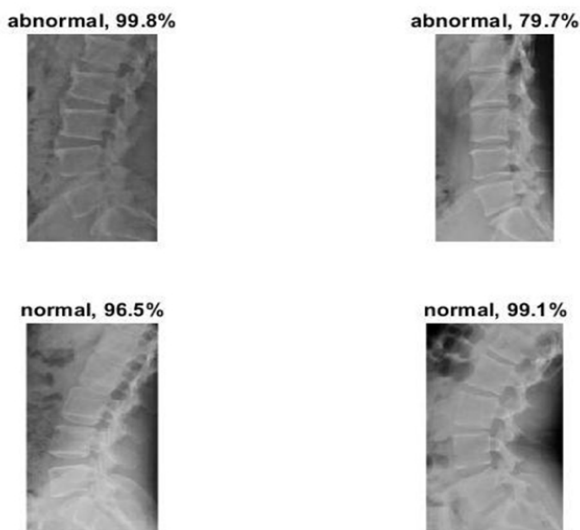
Figure 4. Prediction results from six randomly selected images during testing of the VGG-16 Model
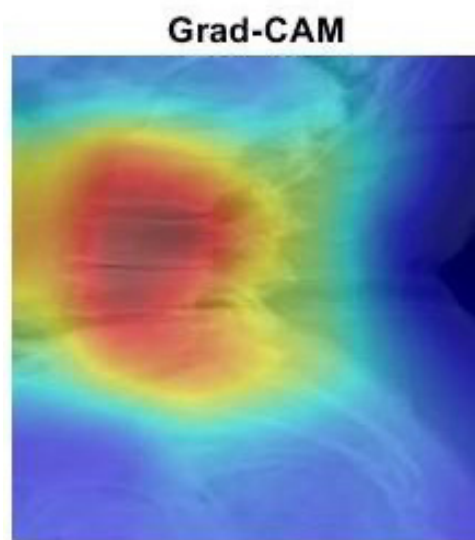
Figure 5. Lateral lumbar radiography image obtained using the Grad-CAM technique

Table 3. Hyperparameters used in ensemble learning	
Classifier	**Parameters**
Bagging	*BaggingClassifier(base_estimator = random_forest, n_estimators=100, random_state= 10)* *RandomForestClassifier(min_samples_leaf= 1, n_estimators=500, max_features = 2, max_depth = 100, bootstrap =True)*
Boosting	*AdaBoostClassifier(DecisionTreeClassifier(max_depth=1), n_estimators=200*
Stacking	*estimators = [('rf', RandomForestClassifier(n_estimators=10, random_state= 2)),* *('knn',KNeighborsClassifier(n_neighbors=5))], Meta_estimator = logistic regression*

DISCUSSION

Plain lateral lumbosacral radiographs were used in this study to diagnose lumbar pathologies, such as disc pathologies, spondylolisthesis, and osteoarthritic changes. The YOLOv4 object detector algorithm was used to eliminate artifacts not required for training the radiographs. The object detector automatically cropped all radiographs to isolate the lumbar and sacral vertebrae, which are the regions of interest. The transfer learning application involved the use of pretrained VGG-16, ResNet-50, and MobileNetV2 networks for object classification. The evaluation of each model's performance was based on metrics such as accuracy, sensitivity, specificity, precision, F1 score, AUC, and Cohen's kappa coefficient.

In distinguishing lumbar vertebral pathologies, identification of abnormal case radiographs using features selected using a threshold value from features extracted by processing the intermediate layer of VGG-16 outperformed transfer learning
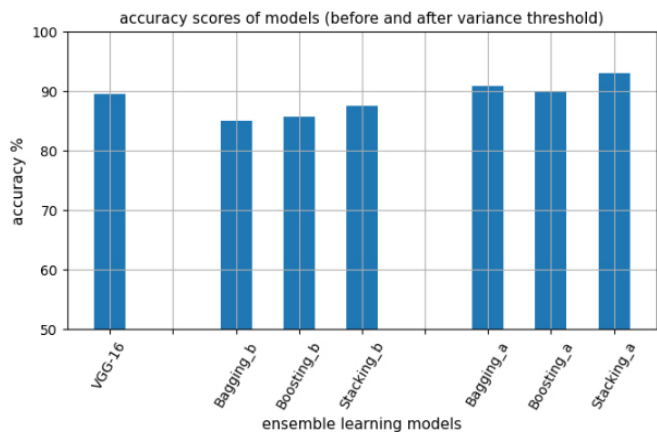
"b" stands for before feature selection, "a" stands for after feature selection

Figure 6. Performance scores of the ensemble learning models
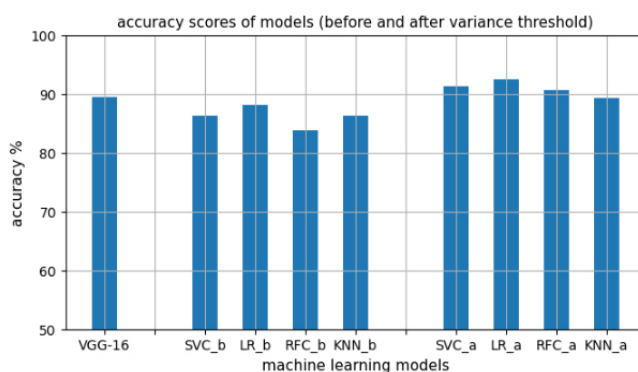
Figure 7. Performance scores of the machine learning models SVC: Support vector classifier, LR: Logistic regression, RFC: Random forest classifier, KNN: k-nearest neigbors, b: Before feature selection, a: After feature selection

Table 4. Performance metrics of ensemble learning algorithms

Feature selection	Classifier	Accuracy (%)	Sensitivity (%)	Specificity(%)	Precision (%)	F1 score (%)	AUC	Cohen's kappa
Before	**Bagging**	85.0	77.6	90.4	85.2	81.2	0.94	0.68
	Boosting	85.7	85.0	86.1	81.1	83.2	0.93	0.70
	Stacking	87.5	85.0	89.3	85.0	85.0	0.93	0.74
After*	**Bagging**	90.9	88.3	93.1	91.5	89.9	0.97	0.81
	Boosting	89.8	91.8	88.2	86.8	89.2	0.97	0.79
	Stacking	93.0	91.8	94.1	92.9	92.3	0.97	0.86
*After feature selection with variance threshold: 0.01, AUC: Area under the curve								

Table 5. Hyperparameters used in machine learning

Classifier	Parameters
RF	*RandomForestClassifier(n_jobs=-1, class_weight='balanced', max_depth= 5, random_state=41)*
SVM	*SVC(probability=True), default parameters*
LR	*LogisticRegression(solver='lbfgs', max_iter=500, random_state=12)*
KNN	*KNeighborsClassifier(n_neighbors= 4)*
RF: Random forest, SVM: Support vector machine, LR: Logistic regression, KNN: k-nearest neighbors, SVC: Support vector classifier	

Table 6. Machine learning algorithm performance metrics before and after feature selection

Feature selection	Classifier	Accuracy (%)	Sensitivity (%)	Specificity (%)	Precision (%)	F1 score (%)	AUC	Cohen's kappa
Before	**SVC**	86.3	82.0	89.3	84.6	83.3	0.94	0.71
	LR	88.1	85.0	90.4	86.3	85.7	0.95	0.75
	RFC	83.8	82.0	85.1	79.7	80.8	0.93	0.66
	KNN	86.3	76.1	93.6	89.4	82.2	0.93	0.71
After*	**SVC**	91.2	90.4	91.9	90.4	90.4	0.96	0.82
	LR	92.5	93.1	91.9	90.6	91.8	**0.97**	0.84
	RFC	90.6	89.0	91.9	90.2	89.6	0.96	0.81
	KNN	89.3	82.1	**95.4**	**93.7**	87.5	0.96	0.78

*After feature selection with variance threshold: 0.01, SVC: Support vector classifier, LR: Logistic regression, RFC: Random forest classifier, KNN: k-nearest neighbors
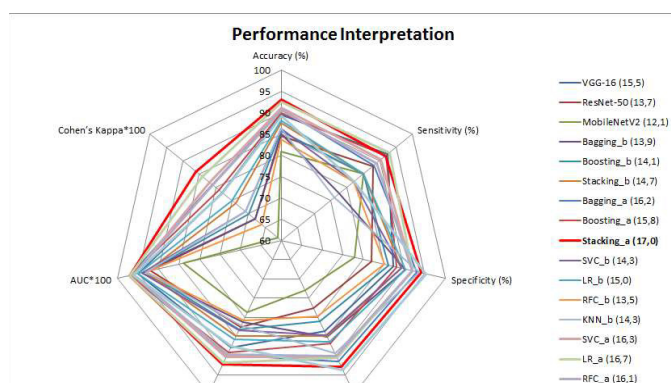

Figure 8. Performances of the models. Area of each shape is shown in parenthesis
SVC: Support vector classifier, LR: Logistic regression, RFC: Random forest classifier, KNN: k-nearest neigbors, b: Before feature selection, a: After feature selection

models using pre-trained networks, such as VGG-16, ResNet-50, and MobileNetV2, and learning methods that do not apply feature selection. The results from the ensemble learning model with the stacking classifier using features selected using a threshold value of 0.01 from the extracted features were as follows: accuracy, 93.0% (best); sensitivity, 91.8%; specificity, 94.1%; precision, 92.9%; F1 score, 92.3% (best); AUC, 0.97 (one of the best); and Cohen's kappa, 0.86 (best). The results from machine learning model with KNN classifier using the same selected features set were: accuracy 89.3%, sensitivity 82.1%, specificity 95.4% (best), precision 93.7% (best), F1 score 87.5%, AUC 0.96, and Cohen's kappa 0.78 and the results from machine learning model with LR classifier using the same set were: accuracy 92.5%, sensitivity 93.1% (best), specificity 91.9%, precision 90.6%, F1 score 91.8%, AUC 0.97 (one of the best), and Cohen's kappa 0.78.

Many successful studies have been conducted on plain radiographs using deep learning methods. Üreten et al. (27) studied normal (n=290) and sacroiliitis pelvic radiographs (n=295), in which pre-trained VGG-16 ResNet-101 and Inception-101 architectures were used for the deep learning models. The test images yielded 89.9%, 90.9%, 88.9%, 88.9%, and 0.96 for the accuracy, sensitivity, specificity, precision, and AUC performance measures, respectively (27). Another study by Üreten et al. (9) evaluated hip osteoarthritis using a transfer learning application with the VGG-16 network, using 221 normal hip X-rays and 213 osteoarthritis hip X-rays. Values of 90.2%, 97.6%, 83.0%, and 84.7% were obtained for the accuracy, sensitivity, specificity, and 84.7%, respectively (9).

Cina et al. (28) achieved success with absolute median errors of 1.84°, 2.43°, and 1.98° for the L1-L5, L1-S1, and SS angles, respectively, using a deep learning model for the localization of thoracolumbar vertebrae using 10,193 images. Another study based on a deep learning model using a total of 871 images, consisting of 413 X-ray and 458 magnetic resonance imaging (MRI), in which lumbar vertebral imaging findings were evaluated using MRI and X-ray in patients with low back pain, values of 97% for specificity, 94% for sensitivity, and 0.98 for AUC performance were obtained (29). Studies have also been conducted to determine the lumbar lordosis angle (30,31) and lumbar spondylolisthesis using plain radiographs with the deep learning method (32,33). Deep learning has also been applied to detect vertebral compression fractures (34,35).

One of the review articles on deep-learning studies using lumbar, cervical, and thoracic vertebral images conducted between 2006 and 2020 stated that deep-learning methods have enormous potential and can help clinical staff improve the level of medical care, increase work efficiency, and reduce the incidence of adverse events (36).

Maraş et al. Computerized Diagnosis of Low Back Pain

Rheumatology Quarterly 2024;2(3):121-9

A deep learning approach and the VGG-16 architecture were used to analyze 161 normal and 170 lateral cervical radiographs of osteoarthritis and degenerative disc disease in a previous study. The study has an accuracy of 93.9%, sensitivity of 95.8%, specificity of 92.0%, and precision of 92.0%. In that study, pre-processing was performed manually, and regions that were not necessary for training due to the noise they contained were clipped from each radiograph (37). Deep learning-based object detection utilizes the R-CNN family, single-shot detector, and YOLO algorithms (11,21,38). In this study, the YOLOv4 algorithm was trained on 30 lumbar radiographs. With this model, radiographs were automatically cropped, and regions that were not required for training and that could adversely affect the results were removed. Thus, an end-to-end model was obtained, and classification was then performed on the radiographs.

In the present study, we applied transfer learning methods using pre-trained VGG-16, ResNet-50, and MobileNetV2 networks. Although transfer learning methods allow training on fewer data (39,40), overfitting is a fundamental problem. In our study, dropout, learning rate decay, L2 regularization, and early stopping were applied to prevent overfitting, and we did not observe overfitting in the training-test graphics and results. When deep learning methods are used, it is not known which features the method learns (black box). Hence, heat maps can be created using the GradCAM method to determine which region of the image the deep learning algorithm is recognizing; this technique highlights regions that are important in the decisions made by the model (25,26). In this study, Grad-CAM techniques were used to create heatmaps.

The use of imaging methods has become more frequent in recent years because radiologists cannot evaluate plain radiographs in most centers because of workload pressures. Machine learning and deep learning models offer ways to help clinicians in this regard. To develop models suitable for clinical use, multicenter studies using a large number of radiographs are needed. The limitations of this study include the small number of radiographs and the fact that classification was conducted using radiographs obtained from a single center.

Many pathologies are related to low back pain, heavy lifting, muscle and ligament tension due to sudden movements, degenerative disc pathologies, osteoarthritic changes, skeletal disorders such as scoliosis and spondylolisthesis, as well as fibromyalgia. The proposed method is helpful for diagnosing pathologies that can be detected by plain radiography. However, it cannot be used to diagnose fibromyalgia, which is an essential cause of low back pain. The diagnosis of fibromyalgia is based on the patient's information as well as the presence of trigger points (41).

The performance of the deep learning methods improved as the number of images increased. If studies were conducted on images obtained from different centers and with different X-ray devices, it would be possible to generalize the developed model.

CONCLUSION

This study investigated the possibilities of improving the performance of machine learning methods via feature selection with variance thresholding. The proposed model appears promising because it can assist clinicians in evaluating plain radiographs, which is a promising first step in the management of lower back pain.

Footnote

Ethics Committee Approval: The study was obtained from the University of Health Sciences Turkey, Ankara Bilkent City Hospital Clinical Research Ethics Committee for the study (date: 09/03/2022, number: E1-22-2546).

Informed Consent: Since this study included retrospective research on archive radiographs and did not publish the patients' personal information, obtaining consent forms was unnecessary.

Authorship Contributions

Concept: Y.M., S.D., K.O., E.A., K.Ü., H.H.M., Design: Y.M., A.K., S.D., K.O., E.A., E.S.S., K.Ü., H.H.M., Data Collection or Processing: Y.M., A.K., S.D., E.S.S., K.Ü., H.H.M., Analysis or Interpretation: Y.M., K.Ü., H.H.M., Literature Search: Y.M., A.K., S.D., K.O., E.A., E.S.S., Writing: Y.M., A.K., E.S.S., K.Ü., H.H.M.

Conflict of Interest: The authors have no conflicts of interest to declare.

Financial Disclosure: The authors declared that this study received no financial support.

REFERENCES

1. Hoy D, Brooks P, Blyth F, et al. The epidemiology of low back pain. Best Pract Res Clin Rheumatol. 2010;24:769-81.

2. Kerry S, Hilton S, Dundas D, et al. Radiography for low back pain: a randomised controlled trial and observational study in primary care. Br J Gen Pract. 2002;52:469-74.

3. Raastad J, Reiman M, Coeytaux R, et al. The association between lumbar spine radiographic features and low back pain: a systematic review and meta-analysis. Semin Arthritis Rheum. 2015;44:571-85.

4. Lindsey R, Daluiski A, Chopra S, et al. Deep neural network improves fracture detection by clinicians. Proc Natl Acad Sci USA. 2018;115: 11591-6.

Rheumatology Quarterly 2024;2(3):121-9

Maraş et al. Computerized Diagnosis of Low Back Pain

5. Lim J, Kim J, Cheon S. A deep neural network-based method for early detection of osteoarthritis using statistical data. Int J Environ Res Public Health. 2019;16:1281.

6. Cheng CT, Ho TY, Lee T, et al. Application of a deep learning algorithm for detection and visualization of hip fractures on plain pelvic radiographs. Eur Radiol. 2019;29:5469-77.

7. Ho-Le TP, Center JR, Eisman JA, et al. Prediction of hip fracture in post-menopausal women using artificial neural network approach. Annu Int Conf IEEE Eng Med Biol Soc. 2017;2017:4207-10.

8. Badgeley MA, Zech JR, Oakden-Rayner L, et al. Deep learning predicts hip fracture using confounding patient and healthcare variables. NPJ Digit Med. 2019;2:31.

9. Üreten K, Arslan T, Gültekin KE, et al. Detection of hip osteoarthritis by using plain pelvic radiographs with deep learning methods. Skeletal Radiol. 2020;49:1369-74.

10. He K, Zhang X, Ren S, et al. Deep residual learning for image recognition. In proceeding of the 2016 IEEE Conference on Computer Vision and Pattern Recognition (CVPR); IEEE Computer Society. Las Vegas, NV, USA: 2016.

11. Bochkovskiy A, Wang CY, Liao HYM. YOLOv4: Optimal speed and accuracy of object detection. 2020.

12. Litjens G, Kooi T, Bejnordi BE, et al. A survey on deep learning in medical image analysis. Med Image Anal. 2017;42:60-88.

13. Greenspan H, van Ginneken B, Summers RM. Guest editorial deep learning in medical imaging: Overview and future promise of an exciting new technique. Institute of Electrical and Electronics Engineers Transactions on Medical Imaging. 2016;35:1153-9.

14. Anwar SM, Majid M, Qayyum A, et al. Medical image analysis using convolutional neural networks: a review. J Med Syst. 2018;42:226.

15. Üreten K, Maraş HH. Automated classification of rheumatoid arthritis, osteoarthritis, and normal hand radiographs with deep learning methods. J Digit Imaging. 2022;35:193-9.

16. Krizhevsky A, Sutskever I, Hinton GE. ImageNet classification with deep convolutional neural networks. Communications of the Association for Computing Machinery. 2017;60:84-90.

17. Szegedy C, Liu W, Jia Y, et al. Going deeper with convolutions. In: prooceding of the 2015 IEEE Conference on Computer Vision and Pattern Recognition (CVPR). Boston, MA, USA: IEEE; 2015.

18. Simonyan K, Zisserman A. Very deep convolutional networks for large-scale image recognition. 2014.

19. Howard AG, Zhu M, Chen B, et al. MobileNets: Efficient convolutional neural networks for mobile vision applications. 2017.

20. Huang G, Liu Z, Van Der Maaten L, et al. Densely connected convolutional networks. In: prooceding at the 2017 IEEE Conference on Computer Vision and Pattern Recognition (CVPR); Honolulu, HI, USA: 2017.

21. Aly GH, Marey M, El-Sayed SA, et al. YOLO based breast masses detection and classification in full-field digital mammograms. Comput Methods Programs Biomed. 2021;200:105823.

22. Singh S, Ahuja U, Kumar M, et al. Face mask detection using YOLOv3 and faster R-CNN models: COVID-19 environment. Multimed Tools Appl. 2021;80:19753-68.

23. Nie Y, Sommella P, O'Nils M, et al. Automatic detection of melanoma with Yolo deep convolutional neural networks. In: proceeding at the 2019 E-Health and Bioengineering Conference (EHB); Iasi, Romania: 2019.

24. Raihan-Al-Masud M, Mondal MRH. Data-driven diagnosis of spinal abnormalities using feature selection and machine learning algorithms. PLoS One. 2020;15:e0228422.

25. Selvaraju RR, Cogswell M, Das A, et al. Grad-CAM: Visual explanations from deep networks via gradient-based localization. In: proceeding at the 2017 IEEE International Conference on Computer Vision Venice, Italy: (ICCV); 2016.

26. Chattopadhay A, Sarkar A, Howlader P, et al. Grad-CAM++: Generalized gradient-based visual explanations for deep convolutional networks. In: proceeding at the 2018 IEEE Winter Conference on Applications of Computer Vision (WACV); Lake Tahoe. NV. USA: 2018.

27. Üreten K, Maraş Y, Duran S, et al. Deep learning methods in the diagnosis of sacroiliitis from plain pelvic radiographs. Modern Rheumatol. 2021;33:202-6.

28. Cina A, Bassani T, Panico M, et al. 2-step deep learning model for landmarks localization in spine radiographs. Sci Rep. 2021;11:9482.

29. Tan WK, Hassanpour S, Heagerty PJ, et al. Comparison of natural language processing rules-based and machine-learning systems to identify lumbar spine imaging findings related to low back pain. Acad Radiol. 2018;25:1422-32.

30. Cho BH, Kaji D, Cheung ZB, et al. Automated measurement of lumbar lordosis on radiographs using machine learning and computer vision. Global Spine J. 2020;10:611-8.

31. Kitamura G. Hanging protocol optimization of lumbar spine radiographs with machine learning. Skeletal Radiology. 2021;50:1809-19.

32. Nguyen TP, Chae DS, Park SJ, et al. Deep learning system for Meyerding classification and segmental motion measurement in diagnosis of lumbar spondylolisthesis. Biomed Signal Process Control. 2021;65:102371.

33. Saravagi D, Agrawal S, Saravagi M, et al. Diagnosis of lumbar spondylolisthesis using optimized pretrained CNN models. Comput Intell Neurosci. 2022;2022:7459260.

34. Seo JW, Lim SH, Jeong JG, et al. A deep learning algorithm for automated measurement of vertebral body compression from X-ray images. Sci Rep. 2021;1113732.

35. Kim DH, Jeong JG, Kim YJ, et al. Automated vertebral segmentation and measurement of vertebral compression ratio based on deep learning in X-ray images. J Digit Imaging. 2021;34:853-61.

36. Ren G, Yu K, Xie Z, et al. Current applications of machine learning in spine: From clinical view. Global Spine J. 2020;12:1827-40.

37. Maraş Y, Tokdemir G, Üreten K, et al. Diagnosis of osteoarthritic changes, loss of cervical lordosis, and disc space narrowing on cervical radiographs with deep learning methods. Jt Dis Relat Surg. 2022;33:93-101.

38. Cheng R. A survey: Comparison between Convolutional Neural Network And YOLO in image identification. J Phys Conf Ser. 2020:1453.

39. Gong Y, Luo J, Shao H, et al. A transfer learning object detection model for defects detection in X-ray images of spacecraft composite structures. Compos Struct. 2022;284:115136.

40. Tian Y, Wang J, Yang W, et al. Deep multi-instance transfer learning for pneumothorax classification in chest X-ray images. Med Phys. 2022;49:231-43.

41. Staud R. Evidence for shared pain mechanisms in osteoarthritis, low back pain, and fibromyalgia. Curr Rheumatol Rep. 2011;13:513-20.

ORIGINAL ARTICLE

THE EFFECTS OF MICROALBUMINURIA AND INFLAMMATORY MARKERS ON CAROTIS INTIMA MEDIA THICKNESS IN FAMILIAL MEDITERRANEAN FEVER

Tufan Murat Coşkun[1], Barış Gündoğdu[2], Sema Basat[3]

[1]Medipol University Pendik Hospital, Department of Internal Medicine, İstanbul, Turkey
[2]University of Health Sciences Turkey, Sultan 2. Abdulhamid Han Training and Research Hospital, Clinic of Rheumatology, İstanbul, Turkey
[3]University of Health Sciences Turkey, Ümraniye Training and Research Hospital, Clinic of Internal Diseases, İstanbul, Turkey

Abstract

Aim: This study aimed to investigate the presence of early atherosclerosis due to inflammation and its relationship with microalbuminuria in newly diagnosed Familial Mediterranean fever (FMF) patients.

Material and Methods: Seventy-seven FMF patients who were newly diagnosed and 34 healthy volunteers were enrolled in this study. In all study groups, microalbuminuria in 24 hours urine sample, C-reactive protein (CRP), hemogram, erythrocyte sedimentation rate (ESR), fibrinogen, routine biochemistry, and lipid panels were performed. Carotid intima media thickness (IMT) was measured in both groups using the same ultrasonography device using a 12 MHz linear probe. To minimize technical errors, patients were also evaluated by the same radiologist. In all patients, both the main carotid arteries and internal carotid arteries were examined for morphology.

Results: IMT, triglyceride, high-density lipoprotein, low-density lipoprotein, and cholesterol levels did not differ significantly between the groups (p>0.05). The fibrinogen levels of the FMF group were significantly higher (p<0.01). The CRP levels of the FMF group were significantly higher (p<0.05). On the other hand, ESR, red blood cell, hematocrit, hemoglobin, platelet, and microalbumin measurements did not show statistically significant difference according to the groups (p>0.05). The positive 15.2% correlation between IMT and fibrinogen levels was not statistically significant (r=0.152; p=0.109; p>0.05). There was no statistically significant relationship between IMT and CRP and ESR levels. The negative 10.2% difference between IMT and microalbumin values was not statistically significant (r=-0.102; p=0.289; p>0.05).

Conclusion: The significant difference between the inflammatory markers, such as fibrinogen and CRP between FMF patients and the healthy controls demonstrates that subclinical inflammation continued in the patient group, even if the patient did not develop FMF attack. Although microalbuminuria is known to be an early diagnostic criterion of atherosclerosis, no correlation was detected between microalbuminuria and inflammatory markers and carotid IMT. In summary, since no remarkable correlation was found between FMF-related inflammation and carotid IMT, we do not recommend clinical follow-up with carotid Doppler ultrasound in addition to routine outpatient controls.

Keywords: Familial Mediterranean fever, microalbuminuria, carotid intima media thickness, subclinical inflammation

Rheumatology Quarterly 2024;2(3):130-6

Coşkun et al. Microalbuminuria and Cim Thickness in the FMF Group

INTRODUCTION

Familial Mediterranean fever (FMF) is an autosomal recessive disease that affects especially the Sephardic Jews, Arabs, Turks, and Armenians settled around the Eastern Mediterranean (1). Recurrent fever, peritonitis, pleuritis, arthritis, pericarditis and skin findings are observed. Attacks usually occur in late childhood and adolescence. In 60-70% of the cases, symptoms were observed in the first 10 years, in 80-90% of the cases before the age of 20 years. The mean age at onset was 4.5 years (2).

Several factors have been implicated in the etiopathogenesis of FMF. In FMF, mutations in the Mediterranean fever gene disrupt the structure of the pyrin /marnostrin molecule, resulting in increased leukocyte migration to serosas and a prolonged and inappropriate response to inflammatory stimulation. Thus, acute phase reactants, such as C-reactive protein (CRP), serum amyloid A (SAA), and the erythrocyte sedimentation rate (ESR), are increased in patients with FMF. In this context, studies on the cytokines responsible for acute phase responses were performed, and mediators such as interleukins-1,8 and tumor necrosis factor-alpha were found to be high during the attack periods. In other words, FMF is a chronic inflammation-associated disease, and amyloidosis development is indispensable in patients who do not receive effective treatment regularly. Early diagnosis of the disease and its complications is important because the disease emerges at a very young age and has a chronic course. Recently, the relationship between atherosclerosis and inflammation has become a widely accepted clinical condition (3). However, there are contradictory results in the effect of inflammation on the development of atherosclerosis in FMF characterized by chronic inflammation (4-6). There are also reports that microalbuminuria may be a sign of early diagnosis for atherosclerosis (7,8).

Microalbuminuria due to renal involvement in FMF is the most common finding of organ damage. There are no strong and large population-based clinical studies on the role of albuminuria in FMF in the terms of the early diagnosis of concomitant atherosclerosis.

Due to the fact that it is easy to use, safe and inexpensive in the early diagnosis of atherosclerosis, the measurement of the wall thickness of the carotid artery with Doppler ultrasonography (USG) is a frequently used imaging method (9). Therefore, in this study, we evaluated the relationship between carotid artery wall thickness and microalbuminuria for the presence of atherosclerosis in newly diagnosed FMF who are free of symptoms.

MATERIAL AND METHODS

This study included 34 healthy volunteers and 77 patients with FMF who were newly diagnosed according to the Tel Hashomer criteria at internal disease outpatient clinics between 2010 and 2012 and were not yet treated with colchicine. Anamnesis was performed in all cases, and full physical examinations, necessary laboratory tests, and imaging studies were performed. Patients with a history of diabetes mellitus, hypertension, peripheral artery disease, systemic vasculitis, chronic renal failure, nephrotic syndrome, acute or chronic other inflammatory diseases, psychiatric disorders, malignancy, pregnancy, smoking, anti-inflammatory drug use, morbid obesity, and those aged <16 or >65 years were not included in the study.

In all study groups, we assessed microalbuminuria in 24 hours urine samples, CRP, hemogram, ESR, fibrinogen, blood glucose, low-density lipoprotein cholesterol (LDL-C), triglyceride, high-density lipoprotein cholesterol (HDL-C), tests were performed. CRP levels were measured via the nephelometric method (Colter Immage 800, Beckman, USA) in a thin dry tube after centrifugation in serum. ESR levels per hour were analyzed using the Westergren method (Vacuplus ES-120, Turkey). Complete blood count was performed using an automated analyzer (Siemens Advia 2120, Germany) in the hemogram tube for 24 parameters. Fibrinogen levels were determined using the Clauss method (Amax 200, Germany).

Triglyceride levels by glycerol phosphate oxidase method, HDL-C levels by accelerator selective detergent method, LDL-C levels by enzymatic method, and microalbuminuria by immunoturbidimetric method were measured using an auto analyzer (Abbott architect C8000 biochemistry USA).

Carotid intima media thickness (IMT) was measured in both groups. This measurement was performed on the same USG device (Aplio XG, Toshiba, Japan) using a 12-MHz linear probe. For the measurements, patients were visualized in the supine position with their head facing the opposite side of the examined side and the right and left carotid arteries. In all cases, both common carotid arteries (CCA) and internal carotid arteries were examined for morphology. Measurements were made on B-mode images obtained from the posterior wall in the first 1 cm segment of the internal carotid artery and in the proximal region of approximately 1 cm proximal to the carotid bifurcation. The defined measurements were repeated for both carotid arteries. The IMT value was then evaluated by taking into consideration the average of all the measurements. The presence of plaque or stenosis in the carotid system during the examination was also noted. To minimize technical errors, all measurements were performed by a single radiologist. The upper limit of normal for carotid artery IMT was 0.8 mm. Demographic characteristics, metabolic and inflammatory markers, and IMT measurements of both groups were compared. In addition, the correlation between microalbuminuria and inflammatory markers and carotid IMT

Coşkun et al. Microalbuminuria and Cim Thickness in the FMF Group

Rheumatology Quarterly 2024;2(3):130-6

was investigated in patients with FMF. Written informed consent forms were obtained from all participants before the study. This study was approved by the Ümraniye Training and Research Hospital Clinical Research Ethics Committee (approval number: 16914, date: 18.10.2012).

Statistical Analysis

The Number Cruncher Statistical System 2007 & Power Analysis and Sample Size 2008 statistical software (Utah, USA) was used for statistical analysis. Student's t-test was used to compare descriptive statistical methods (mean, standard deviation, median, frequency, ratio), as well as normal distribution of parameters with normal distribution. The Mann-Whitney U test was used to compare parameters that did not show normal distribution. For qualitative data comparison, Fisher's Exact, chi-square test was used. Statistical significance was defined as $p < 0.05$ for all analyses.

RESULTS

Seventy-seven patients with FMF and 34 healthy controls were included in the study. A comparison of the demographic characteristics of the groups is presented in Table 1. A statistically significant intergroup difference was observed ($p < 0.01$). The patients in the FMF group were significantly older.

There was a statistically significant difference in the levels of fibrinogen (Figure 1) and CRP (Figure 2) in the FMF group compared with the control group ($p < 0.01$ and $p < 0.05$, respectively). However, no significant difference was observed between the carotid IMT groups (Table 2).

There was no statistically significant relationship between carotid IMT and fibrinogen levels, although a positive value of 15.2% was detected. In addition, the correlations of carotid IMT with CRP and ESR were not statistically significant. Furthermore, carotid IMT and microalbumin levels were negatively correlated, with a value of 10.2% being not statistically significant. In summary, neither inflammatory markers nor microalbuminuria was correlated with IMT in patients with FMF (Table 3).

DISCUSSION

In this study, when patients with FMF and healthy controls were compared in terms of carotid IMT (surrogate marker of early atherosclerosis), although some inflammatory markers were significantly higher in the FMF group, no significant difference was found between the two groups. There was no correlation between inflammatory markers and carotid IMT. There are very few studies in the literature on this issue. While the present study was consistent with the results of several clinical studies, it was incompatible with the results of other studies.
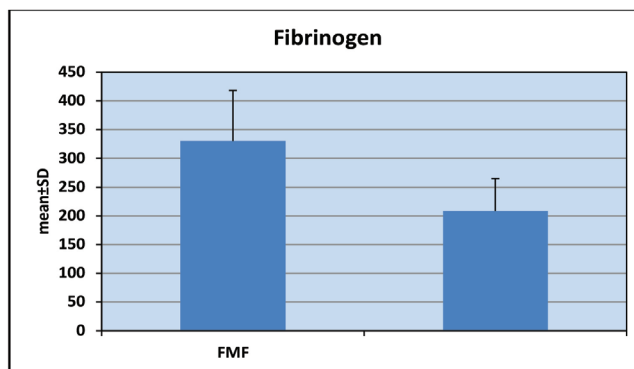

Figure 1. Distribution of fibrinogen levels in the two groups
FMF: Familial Mediterranean fever
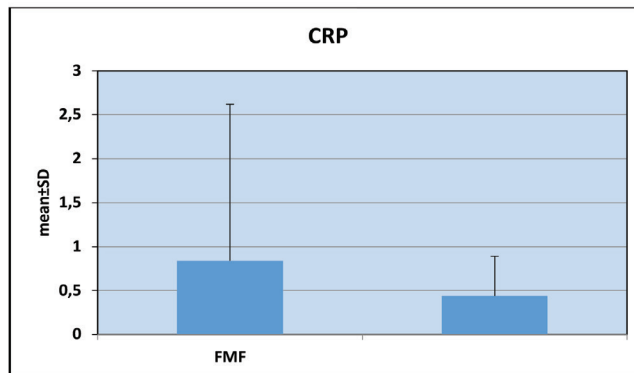
Figure 2. Distribution of CRP levels in both groups
CRP: C-reactive protein

Table 1. Distribution of demographic variables in the two groups			
	FMF (n=77)	**HC (n=34)**	**p-value**
Age (years)	31.71±9.32	41.79±9.93	0.001**
BMI (kg/m²)	26.14±4.99	28.19±3.55	0.032*
ªGender	Males, n (%)	34 (44.2)	10 (29.6)	0.143
	Female, n (%)	43 (55.8)	24 (70.6)	
Student t-test, ªYates test, *p<0.01, **p<0.01. Data presented as mean ± SD and number (percentage), FMF: Familial Mediterranean fever, HC: Healthy controls, BMI: Body mass index, SD: Standard deviation			

Table 2. Distribution of metabolic and inflammatory markers and carotid artery IMT			
	FMF (n=77)	HC (n=34)	p-value
IMT	0.55±0.66	0.54±0.08	0.526
[a]TG; (Median)	121.93±78.88 (102.00)	134.88±64.62 (115.50)	0.099
HDL-C	43.01±12.85	47.09±9.80	0.102
LDL-C	102.86±33.26	111.44±32.79	0.211
TC	170.26±43.25	185.51±36.56	0.076
Fibrinogen	330.32±88.02	208.23±56.48	0.001**
[a]CRP; (Median)	0.84±1.78 (0.39)	0.44±0.45 (0.31)	0.038*
[a]ESR; (Median)	12.77±11.22 (8.00)	10.82±6.60 (10.00)	0.822
WBC	7.41±1.99	7.85±1.89	0.282
HCT	40.11±4.31	38.57±4.16	0.082
Hgb	13.37±2.04	12.48±1.32	0.021
[a]Plt; (Median)	274.96±74.22 (269.00)	315.11±312.53 (262.00)	0.611
[a]Microalbumin; (Median)	14.84±16.70 (8.10)	11.64±7.00 (11.50)	0.920
[b]Plaque Absent, n (%)	66 (85.7%)	34 (100.0%)	0.017*
Present, n (%)	11 (14.3%)	0 (0.0%)	

Student t-test, [a]Mann-Whitney U test, [b]Fisher's Exact test, *p<0.01, **p<0.01. Data presented as mean ± SD and number (percentage), IMT: Intima media thickness, FMF: Familial Mediterranean fever, HC: Healthy controls, HDL-C: High-density lipoprotein cholesterol, LDL-C: Low-density lipoprotein cholesterol, TC: Total cholesterol, CRP: C-reactive protein, ESR: Erythrocyte sedimentation rate, WBC: White blood cell, HCT: Hematocrit, Hgb: Hemoglobin, Plt: Platelet, TG: Triglyceride

Table 3. Evaluation of the correlation between inflammatory markers and microalbuminuria and carotid IMT in patients with FMF		
FMF patients (n=77)	IMT	
	r	p-value
Fibrinogen	0.152	0.109
[a]CRP	0.036	0.705
[a]ESR	0.054	0.574
[a]Microalbumin	-0.102	0.289

r=Pearson correlation, [a]r=Spearman's rho. IMT: Intima media thickness, FMF: Familial Mediterranean fever

Bilginer et al. (4) reported that all acute-phase reactants (ESR, CRP, fibrinogen and SAA) were significantly higher in patients with FMF than in healthy controls, although there was no FMF attack. They found a positive correlation between internal carotid artery IMT and ESR and fibrinogen levels. These findings were consistent with ongoing subclinical inflammation, although no apparent FMF attack was noted. They thought that this subclinical inflammation could explain the increase in carotid IMT detected in patients with FMF. They concluded that suppression of inflammation with adequate doses of colchicine could prevent this complication and recommended measuring carotid IMT to detect early arterial changes in patients with FMF (4).

In a study by Langevitz et al. (10) on patients with FMF receiving colchicine despite treatment, they thought that they would find increased ischemic heart disease due to continuous inflammation. However, as a result of the study, there was no increased incidence of ischemic heart disease in FMF patients. On the contrary, the authors found that the prevalence of ischemic heart disease in patients with FMF decreased by 15.5% compared with the control group. They thought that this was due to the effect of colchicine treatment, which began at a young age and continued for life. These patients were exposed to both inflammatory protective effects and side effects, such as nausea, anorexia, and diarrhea (10). Although, in the study of Langevitz et al. (10) found that ischemic heart disease was lower than expected in adult patients with FMF, we believe that these patients should be followed up objectively.

In a case report by Ordu et al. (11), a patient with acute coronary syndrome (ACS) diagnosed with FMF after 20 years of age partially responded to colchicine treatment. Therefore, they thought that the cause of early ACS in patients may be due to chronic inflammation (11). As in this case, there are clinical studies showing that administration of aspirin to patients with late diagnosis or unresponsive to colchicine treatment and with

Coşkun et al. Microalbuminuria and Cim Thickness in the FMF Group

Rheumatology Quarterly 2024;2(3):130-6

high CRP levels significantly reduces CRP levels, and in parallel, the risk of ischemic events decreases in these patients (12,13).

Therefore, patients with a diagnosis of FMF have a high risk of early ischemic heart disease; suggested that these patients could be followed more frequently by measuring carotid IMT and CRP levels, which are indicators of early atherosclerosis. ACS should be considered in the differential diagnosis of patients with FMF presenting with angina, and patients should be carefully evaluated in this respect.

In a study performed by Akdogan et al. (6) in the same hospital adult population, they found an increased carotid IMT in patients with FMF compared with healthy volunteers, independent of known risk factors for atherosclerosis. At the same time, as expected, acute-phase reactants were found to be high in patients with FMF. It was reported that this change in the IMT of the carotid artery in patients with FMF was due to ongoing inflammation at a low level. In addition, the similarity of serum lipid changes in patients with FMF and other chronic inflammatory diseases, such as rheumatoid arthritis (14). Although they thought that the ongoing inflammation in patients with FMF could cause an increase in carotid IMT due to low HDL-C levels, apart from the disease itself, they did not detect such a situation in the aforementioned study (6). Although low HDL-C levels were observed in our study, no statistically significant difference was found.

As stated earlier, in the study of Peru et al. (5), it was emphasized that environmental factors may play an important role in the emergence of FMF, and FMF patients with the same genetic background may differ according to the region in which they live or their living habits. In this context, a study reported that Armenian-born FMF patients in the USA develop less amyloidosis than FMF patients in Armenia (15). Therefore, the inconsistencies in the results of the studies can be explained by the differences in the lifestyles and socioeconomic status of the patients in the study groups. In this study (5), the carotid artery IMT values of pediatric FMF patients were significantly increased compared with the age- and sex-appropriate healthy control group, which supports the study of Akdogan et al. (6).

In another study conducted by Ugurlu et al. (16), patients with FMF and SLE were investigated. Carotid and femoral artery ITM was increased in both groups. Plaque increase was also detected in patients with SLE, but no increase was observed in patients with FMF. The results of this study are similar to those of other studies (16).

In a study designed by Oren et al. (17), patients with FMF receiving colchicine treatment and individuals in the healthy control group were compared by collecting urine during the day and night when they were active, and no significant difference was found. However, a slight increase was detected in urine collected in the morning compared with the night in the control group. This increase was found to be significantly different in patients with FMF than at night, and this exaggerated response was expressed as a sign of mild glomerular damage in patients with FMF (17). Similarly, Saatci et al. (18) reported an increase in microalbuminuria in exacerbation after colchicine treatment was discontinued in patients diagnosed with FMF.

Microalbuminuria is associated with renal damage and endothelial dysfunction in FMF patients. In another study conducted for this purpose, Güneş et al. (19) measured flow-mediated dilatation (FMD) showing endothelial dysfunction from the left arm brachial artery using Doppler ultrasound and compared it with microalbuminuria and found that this value was lower in FMF patients with microalbuminuria than in patients without microalbuminuria. Therefore, the authors predicted that FMD could be used for the early detection of renal damage and endothelial dysfunction (19).

Furthermore, in a study evaluating early markers of atherosclerosis such as FMD, nitroglycerin-induced endothelium-independent peripheral vasodilation, and CCA IMT in patients with FMF, no abnormalities were found in these parameters when receiving regular daily colchicine therapy (20). In this study, the authors stated that it may be possible that pyrin or any other protein that plays a role in the pathogenesis of FMF may interact with components in the pathogenesis of atherosclerosis and prevent its development. They believed that FMF attacks are unresponsive to other drugs, but their dramatic response to colchicine, which protects against FMF attacks and prevents the development of amyloidosis, may support the idea that the inflammatory process in FMF has a different mechanism from other rheumatological diseases. They argued that inflammation in patients with FMF could be explained by another possible mechanism. Severe inflammation in an FMF attack usually subsides in 3-4 days, but subclinical inflammation continues even when patients use regular colchicine.

However, low inflammation levels may not be sufficient to accelerate the development of atherosclerosis.

In addition, studies have shown that a decrease in urinary glycosaminoglycan (GAG) levels and the development of microalbuminuria may be the findings pointing to the development of amyloidosis in patients with FMF, and that GAG levels will increase and microalbuminuria will regress with increasing colchicine doses (21,22).

Apart from these, it is useful to mention some limitations of our clinical study. First of all, in this study, although high inflammatory

Rheumatology Quarterly 2024;2(3):130-6

Coşkun et al. Microalbuminuria and Cim Thickness in the FMF Group

markers suggest that there is continuous inflammation, there were visible differences in microalbuminuria and carotid IMT between the FMF group and the control group, but these differences were not significant because the study group was not sufficiently large or the disease was newly diagnosed, and the effects of the inflammatory process were observed. This may be due to the fact that not enough time has passed. Similar to some other studies (4-6,18) in a study to be conducted in a larger group, increased carotid IMT may be detected in the FMF group. However, given that this group also started using colchicine, Sari et al. (20), it is possible that no difference was detected due to the protective effect of colchicine.

Second, although plaque was detected in the carotid artery in 11 patients in the FMF group, there was no plaque in the control group, and widespread irregularity was present in 1 patient in whom we detected amyloidosis in this present study, although there was no visible plaque on imaging. The insignificance of this difference may be due to the insufficient number of participants in our study groups.

Third, carotid IMT may have affected the results because the control group was older than the FMF group. The fact that FMF disease is also affected by environmental factors other than genetic factors may be reflected in the results because our patient population consisted of people living in a relatively low socioeconomic environment.

Lastly, we could not investigate the FMF gene mutation in patients in the control group because of the high cost; however, it is possible that there are carriers in this group, and in this case, the results may be affected because such individuals will also have subclinical inflammation.

As mentioned previously, the relationship between microalbuminuria and atherosclerosis has been demonstrated in various studies in the literature. Although this relationship has not yet been proven in patients with FMF, it is highly probable that the vascular problems observed in this group of patients are observed simultaneously with microalbuminuria in patients with this disease and renal involvement. If this relationship is proven, a detailed cardiac evaluation, questioning of other risk factors, and, if necessary, invasive procedures will be performed without loss of time in the microalbuminuria group. In the opposite case; In the FMF patient with a vascular problem, necessary precautions will be taken by looking for microalbuminuria if it has not been done. In order to be clinically guiding, such a relationship must be proven. This requires a larger study group and longer exposure to the effects of FMF disease.

As is well known, patients with renal amyloidosis are at the highest risk of vascular damage. As a result, due to the nature of

FMF, patients with this disease should be considered at increased risk of early vascular changes and atherosclerosis. From this perspective, patients should be evaluated for other inflammatory diseases throughout their lives. For this purpose, our study was important in terms of carotid artery IMT measurement, which is recommended as a non-invasive and early diagnostic method and is predictive of subclinical inflammation, especially in cases of microalbuminuria (23).

CONCLUSION

In summary, we investigated whether there is an increase in carotid IMT due to ongoing inflammation in patients with FMF and whether this condition is associated with microalbuminuria. The significant difference in inflammatory markers, such as fibrinogen and CRP, between our patient population and the control group indicates that subclinical inflammation continues in the patient population, even when the patient is not in an attack. In conclusion, given that no significant correlation was found between inflammation and carotid IMT, we do not recommend regularly ordering carotid Doppler USG in addition to routine outpatient clinic checks due to the cost of providing healthcare services.

Footnote

Authorship Contributions

Surgical and Medical Practices: T.M.C., Concept: S.B., Design: S.B., Data Collection or Processing: T.M.C., Analysis or Interpretation: T.M.C., Literature Search: T.M.C., B.G., Writing: T.M.C.

REFERENCES

1. Sohar E, Gafni J, Pras M, et al. Familial Mediterranean fever. A survey of 470 cases and review of the literature. Am J Med. 1967;43:227-53.

2. Brik R, Shinawi M, Kepten I, et al. Familial Mediterranean fever: clinical and genetic characterization in a mixed pediatric population of Jewish and Arab patients. Pediatrics. 1999;103:70.

3. Libby P. Inflammation in atherosclerosis. Nature. 2002;420:868-74.

4. Bilginer Y, Ozaltin F, Basaran C, et al. Evaluation of intima media thickness of the common and internal carotid arteries with

inflammatory markers in Familial Mediterranean fever as possible predictors for atherosclerosis. Rheumatol Int. 2008;28:1211-6.

5. Peru H, Altun B, Doğan M, et al. The evaluation of carotid intima-media thickness in children with Familial Mediterranean fever. Clin Rheumatol. 2008;27:689-94.

6. Akdogan A, Calguneri M, Yavuz B, et al. Are Familial Mediterranean fever (FMF) patients at increased risk for atherosclerosis? Impaired Endothelial Function and Increased Intima Media Thickness Are Found in FMF. J Am Coll Cardiol. 2006;48:2351-3.

7. Kong X, Jia X, Wei Y, et al. Association between microalbüminuria and subclinical atherosclerosis evaluated by carotid artery intima-media in elderly patients with normal renal function. BMC Nephrol. 2012;13:37.

8. Ozyol A, Yucel O, Ege MR, et al. Microalbüminuria is associated with the severity of coronary artery disease independently of other cardiovascular risk factors. Angiology. 2012;63:457-60.

9. Salonen JT, Salonen R. Ultrasound B-mode imaging in observational studies of atherosclerotic progression. Circulation. 1993;87(Suppl 3):56-65.

10. Langevitz P, Livneh A, Neumann L, et al. Prevalence of ischemic heart disease in patients with Familial Mediterranean fever. Isr Med Assoc J. 2001;3:9-12.

11. Ordu S, Kaya S, Aydın M, et al. A Case of Familial Mediterranean fever who was presented with acute coronary syndrome. Duzce Med J. 2009;11:39-41.

12. Uyarel H, Karabulut A, Ökmen E, et al. Familial Mediterranean fever and acute anterior myocardial infarction in a young patient. Anadolu Kardiyol Derg. 2006;6:272-4.

13. Liuzzo G, Biasucci LM, Gallimore JR, et al. The prognostic value of Creactive protein and serum amyloid a protein in severe unstable angina. N Engl J Med. 1994;331:417-24.

14. Sattar N, McCarey DW, Capell H, et al. Explaining how "high-grade" systemic inflammation accelerates vascular risk in rheumatoid arthritis. Circulation. 2003;16;108:2957-63.

15. Schwabe AD, Peters RS. Familial Mediterranean fever in Armenians. Analysis of 100 cases. Medicine (Baltimore). 1974;53:453-62.

16. Ugurlu S, Seyahi E, Cetinkaya F, et al. Intima-media thickening in patients with Familial Mediterranean fever. Rheumatology (Oxford). 2009;48:911-5.

17. Oren S, Viskoper JR, Ilan S, et al. Urinary albumin excretion in patients with Familial Mediterranean fever: A Pilot Study. Am J Med Sci. 1991;301:375-8.

18. Saatci U, Ozdemir S, Ozen S, et al. Serum concentration and urinary excretion of beta 2-microglobulin and microalbüminuria in Familial Mediterranean fever. Arch Dis Child. 1994;70:27-9.

19. Güneş H, Kıvrak T, Tatlısu M, et al. Relationship between endothelial dysfunction and microalbuminuria in Familial Mediterranean fever. Eur J Rheumatol. 2016;3:61-4.

20. Sari I, Karaoglu O, Can G, et al. Early ultrasonographic markers of atherosclerosis in patients with Familial Mediterranean fever. Clin Rheumatol. 2007;26:1467-73.

21. Baskin E, Saatci U. Microalbuminuria in the course of Familial Mediterranean fever. Nephrol Dial Transplant. 2004;19: 2678.

22. Lobato L, Beirão I, Silva M, et al. Familial ATTR amyloidosis: microalbuminuria as a predictor of symptomatic disease and clinical nephropathy. Nephrol Dial Transplant. 2003;18:532-8.

23. Simon A, Gariepy J, Chironi G, et al. Intima-media thickness: a new tool for diagnosis and treatment of cardiovascular risk. J Hypertens. 2002;20:59-69.

A THROMBOSPONDIN TYPE-1 MOTIF, MEMBER 13 (ADAMTS13) LEVELS DECREASE IN COVID-19 PATIENTS

Umut Aydın[1], Deccane Düzenci[2], Fatih Albayrak[3], Ramazan Fazıl Akkoç[4], Burak Öz[5], Ahmet Karataş[5]

[1]İnönü University Faculty of Medicine, Department of Oncology, Malatya, Turkey
[2]İnönü University Faculty of Medicine, Department of Intensive Care, Malatya, Turkey
[3]Gaziantep City Hospital, Clinic of Rheumatology, Gaziantep, Turkey
[4]Fırat University Faculty of Medicine, Department of Anatomy, Elazığ, Turkey
[5]Fırat University Faculty of Medicine, Department of Rheumatology, Elazığ, Turkey

Abstract

Aim: Thrombotic pathologies develop at an increasing rate in severe acute respiratory syndrome coronavirus 2 (SARS-CoV-2) infection. Understanding the pathologies that cause thrombosis in SARS-CoV-2 infection is important for developing prophylaxis strategies for the development of thrombosis and regulating treatment in cases of thrombosis. For all these reasons, we aimed to evaluate the levels of A disintegrin and metalloproteinase with a Thrombospondin Type-1 Motif Member 13 (ADAMTS13), in SARS-CoV-2 patients.

Material and Methods: The data of patients who were followed up in the intensive care unit due to coronavirus disease of 2019 (COVID-19) with lung involvement, who received respiratory support and pulse steroid therapy, and those who were followed up as outpatients without lung involvement were analyzed. Demographic data, laboratory results, and serum ADAMTS13 levels were recorded. These results were compared with those of the control group.

Results: ADAMTS13 levels were significantly lower in the COVID-19 group without lung involvement than in the control group (p=0.037). ADAMTS13 levels were significantly lower in the COVID-19 group with lung involvement than in the control group (p=0.016). There was no difference in ADAMTS13 levels between COVID-19 patients with and without lung involvement (p=0.797). There was no significant difference in ADAMTS13 levels between patients with and without chronic diseases in the COVID-19 group (p=0.40 for those without lung involvement; p=0.573 for those with lung involvement).

Conclusion: SARS-CoV-2 caused a decrease in ADAMTS13 levels. ADAMTS13 levels were decreased more in patients with lung involvement than in those without lung involvement. Decreased ADAMTS13 levels in COVID-19 may be a cause of the prothrombotic process.

Keywords: COVID-19, ADAMTS13, SARS-CoV-2, trombosis

Address for Correspondence: Ahmet Karataş, Fırat University Faculty of Medicine, Department of Rheumatology, Elazığ, Turkey
Phone: +90 505 588 16 07 **E-mail:** drakaratas@yahoo.com **ORCID ID:** orcid.org/0000-0002-6725-4182

Aydın et al. ADAMTS13 Levels in COVID-19 Patients

Rheumatology Quarterly 2024;2(3):137-43

INTRODUCTION

In 2019, severe acute respiratory syndrome coronavirus 2 (SARS-CoV-2) was identified as a novel coronavirus. In 2020, SARS-Cov-2 was declared a pandemic by the World Health Organization. The disease has spread rapidly worldwide, causing over 1.1 million deaths, and the number of cases and deaths is steadily increasing (1). The clinical presentation of patients with coronavirus disease of 2019 (COVID-19) may be asymptomatic, or some patients may progress to a more serious and systemic disease characterized by treatment-resistant fever, acute respiratory distress syndrome (ARDS) and acute lung injury. In addition, shock and multiple organ dysfunction are associated with significant mortality may develop (2-4).

Infections can trigger the development of autoimmune diseases. Therefore, it is important to understand the interaction between viral infections and immunogenic events. Rheumatologists are often involved in COVID-19 treatment management. The incidence of thrombosis increases in systemic inflammation and infectious diseases.

However, Helms et al. (5) among patients admitted to the intensive care unit with a diagnosis of ARDS, a higher thrombosis rate was found in patients with COVID-19-associated ARDS compared with those with non-COVID-19-associated ARDS. Predisposition to thrombosis that can be detected in many coronavirus patients has been termed coronavirus-associated coagulopathy. Coronavirus-associated coagulopathy may manifest itself as increased D-Dimer levels, increased prothrombin time, and decreased platelet counts (6).

A Thrombospondin Type-1 Motif, Member 13 (ADAMTS13) is a zinc-containing metalloproteinase enzyme that degrades von Willebrand factor (vWF). ADAMTS13 is not stored in cells but is secreted directly out of cells from the Golgi apparatus after synthesis. The release is constant and regular (7). If there is a decrease in the amount or activity of ADAMTS13, the breakdown of vWF into small fragments cannot occur. Large vWF multimers adhere to the endothelium and form chains. In microcirculation, in which circulation is slower, platelet aggregates are formed by the binding platelets to vWF multimers (8,9).

During acute inflammation and/or infection, ADAMTS13 synthesis may decrease due to the secretion of inflammatory cytokines. Indeed, Cao et al. (10) showed that interferon-gamma, interleukin (IL)-4 and tumor necrosis factor-alpha (TNF-α) inhibited ADAMTS13 synthesis without affecting vWF secretion. As a result, in the presence of inflammation, the degradation of vWF multimers is impaired, predisposing them to thrombosis (11).

The aim of this study was to determine ADAMTS13 levels in patients with SARS-CoV-2 infection with lung involvement who received steroid treatment and in patients without lung involvement who did not receive corticosteroid treatment.

MATERIALS AND METHODS

Approval for the study was obtained from the Fırat University Non-interventional Research Ethics Committee (approval number: 2021-3769, dated: 22.09.2021). The study groups consisted of 30 patients with pulmonary involvement who received pulse steroid therapy and 30 patients without pulmonary involvement diagnosed with COVID-19 according to the Republic of Turkey Ministry of Health COVID-19 diagnosis and treatment guidelines and 30 controls (12,13). Disintegrin and metalloproteinase with ADAMTS13 levels in serum samples from COVID-19 patients and healthy controls were assessed by Enzyme-Linked Immunosorbent Assay (ELISA) using the Human ADAMTS13 ELISA Kit obtained from Bioassay Technology Laboratory (Shanghai, China) in accordance with the study procedures specified in the manufacturer's catalog (catalog number: E3484Hu). The assay range of the kit was 0.05-15 ng/mL-15 ng/mL and the minimum measurable level (sensitivity) was 0.025 ng/mL. In addition, the Intra-Assay: CV value of the kit was <8%, whereas the Inter-Assay: CV value was <10%.

Demographic, clinical, and laboratory data of the patients were recorded. Patients were examined for thrombotic thrombocytopenic purpura (TTP) and Hemolytic Uremic Syndrome, and these diseases were excluded. Written informed consent was obtained from the patients or their legal representatives.

Statistical Analysis

The Statistical Package for Social Sciences version 22.0 package program was used to analyze the data obtained. The conformity of the data to the normal distribution was analyzed by Kolmogorov-Smirnov test. Continuous variables with normal distribution were analyzed using the independent samples t-test, and continuous variables without normal distribution were analyzed using the Mann-Whitney U test. Data are presented as mean ± standard deviation. p-values below 0.05 were considered statistically significant.

RESULTS

The mean ages of the patients included in the study was 57.12±14.96 years in the COVID-19 group without lung involvement and 66.93±10.46 years in the COVID-19 group with lung involvement. Gender distribution was similar between

Rheumatology Quarterly 2024;2(3):137-43

Aydın et al. ADAMTS13 Levels in COVID-19 Patients

the groups. When patients diagnosed with COVID-19 were compared with the control group, ADAMTS13 was found to be lower in patients diagnosed with COVID-19 than in the control group (p=0.006) (Table 1). When the groups were compared, the ADAMTS13 level was lower in the COVID-19 group without lung involvement than in the control (p=0.037) (Table 2). In the COVID-19 group with lung involvement, ADAMTS13 levels were lower than those in the control group (p=0.016). ADAMTS13 levels were lower in the COVID-19 group with lung involvement than in the outpatient COVID-19 group, but there was no statistical significance (p=0.797) (Table 1). When the ADAMTS13 levels were compared, they were lower in the non-survivors than in the survivors, but no significant difference was found (p=0.110) (Table 3).

Lymphocyte counts were lower in the COVID group with lung involvement (p=0.003). However, leukocyte counts were higher with neutrophil dominance in the covid group with lung involvement (p<0.001). D-Dimer levels were higher in the covid group with lung involvement (p=0.011), fibrinogen levels were higher in the covid group with lung involvement (p=0.865) and international normalized ratio was higher in the covid group with lung involvement (p=0.362). Among the infectious parameters, C-reactive protein was higher in the COVID group with lung involvement (p<0.001) and procalcitonin was higher in the COVID group with lung involvement (p=0.560) (Table 4).

Clinical and laboratory data for patients with COVID-19 with lung involvement according to the presence of chronic disease are presented in Table 5.

There were no clinical thrombosis findings or data detected in the COVID-19 group with or without lung involvement. When the groups were analyzed in terms of the presence of chronic diseases, 13.3% of the group without lung involvement had hypertension and 13.3% had hypertension and diabetes. In the lung involvement group, 20%, 16.6%, 16.6%, and 3.3% had hypertension, 16.6% had hypertension and ischemic heart disease, 6.6% had hypertension and chronic obstructive pulmonary disease, and 3.3% had hypertension and chronic renal failure. In patients with COVID-19 with lung involvement, the ADAMTS13 level was higher in patients with chronic disease, but the difference was not statistically significant difference (p=0.573) (Table 5).

In patients with COVID-19 without lung involvement, ADAMTS13 levels and laboratory parameters were evaluated in terms of chronic disease, and no statistically significant difference was observed (Table 6).

DISCUSSION

In this study, we investigated the ADAMTS13 levels in patients with SARS-CoV-2 infection without pulmonary involvement and those with pulmonary involvement who were followed up in

Table 1. Age, sex, and ADAMTS13 data of all COVID patients versus controls

	Control (n=30)	COVID-19 (n=60)	p-value
Age (years)	45.89	61.53	<0.001
Gender (Male/Female)	15/15	30/30	0.035
ADAMTS13, ng/mL	1.26±0.72	0.89±0.53	0.006
ADAMTS13: A Thrombospondin Type-1 Motif, Member 13, COVID-19: Coronavirus disease of 2019			

Table 2. Age, sex, and ADAMTS13 level in the control and COVID groups

	Control (n=30)	COVID-19 without lung involvement (n=30)	COVID-19 with lung involvement (n=30)	P1	P2	P3
Age (years)	45.89±17.199	57.12±14.96	66.93±10.46	0.009	0.001	0.006
Gender (Male/Female)	15/15	15/15	15/15	0.177	0.185	0.897
ADAMTS13, ng/mL	1.26±0.72	0.91±0.58	0.87±0.49	0.037	0.016	0.797
P1: Control and COVID group without lung involvement, P2: Control and COVID group with lung involvement, P3: COVID group without lung involvement and covid group with lung involvement, ADAMTS13: A Thrombospondin Type-1 Motif, Member 13, COVID-19: Coronavirus disease of 2019						

Table 3. ADAMTS13 levels between non-survivors and survivors in the COVID-19 group

	Non-survivors (n=24)	Survivors (n=36)	p-value
ADAMTS13, ng/mL	0.77±0.44	0.98±0.59	0.110
ADAMTS13: A Thrombospondin Type-1 Motif, Member 13, COVID-19: Coronavirus disease of 2019			

Table 4. Laboratory data in the COVID-19 group without and with lung involvement

	COVID-19 without lung involvement (n=30)	COVID-19 with lung involvement (n=30)	p-value
HGB, gr/dL	13.69±1.81	12.97±2.27	0.195
Lym, $10^3/\mu L$	1.14±0.56	0.75±0.33	0.003
Neu, $10^3/\mu L$	3.54±2.28	8.25±4.21	0.000
PLT, $10^3/\mu L$	186.17±54.31	209.85±93.06	0.246
WBC, $10^3/\mu L$	5.13±2.39	9.67±4.35	0.000
ALT, µ/L	28.12±15.16	72.22±130.94	0.082
AST, µ/L	32.26±14.24	113.63±248.77	0.090
CRP, mg/dL	29.70±30.22	162.55±125.10	0.000
DD, ng/mL	0.80±0.52	2.57±3.29	0.011
Ferritin, mL/ng	215.00±162.96	598.93±431.57	0.005
Fibrinogen, mg/dL	4.69±0.97	4.82±2.33	0.865
INR	1.01±0.06	1.05±0.15	0.362
Cre, mg/dL	0.97±0.20	1.38±1.44	0.148
Procalcitonin, ng/mL	0.061±0.028	3.72±12.22	0.560
Urea, mg/dL	35.15±14.36	68.10±41.72	0.000

HGB: Hemoglobin, Lym: Lymphocyte, Neu: Neutrophil, PLT: Trombocyte, WBC: White blood cell count, ALT: Alanine aminotransferase, AST: Aspartate aminotransferase, CRP: C-reactive protein, DD: D-Dimer, INR: International normalized ratio, Cre: Creatinine, LDH: Lactate dehydrogenase

Table 5. Variation of parameters among patients with covid-19 and lung involvement receiving pulse steroid depending on the presence or absence of chronic disease.

	Chronic disease is absent (n=8)	Chronic disease is present (n=22)	p-value
ADAMTS13, ng/mL	0.81±0.55	0.91±0.45	0.573
Age (years)	63.38±12.23	68.42±9.59	0.261
Clinical hospitalization days	7.13±14.55	1.74±3.66	0.136
Symptom duration	31.00±14.94	20.53±9.64	0.039
HGB, gr/dL	13.17±0.69	12.88±2.70	0.773
Lym, $10^3/\mu L$	0.66±0.18	0.79±0.37	0.366
PLT, $10^3/\mu L$	239.63±111.84	197.32±84.17	0.289
WBC, $10^3/\mu L$	8.56±3.80	10.14±4.58	0.399
AST, µ/L	75.75±47.63	129.57±295.98	0.617
ALT, µ/L	55.87±18.89	79.10±156.40	0.682
CRP, mg/dL	192.83±129.12	149.80±124.68	0.425
DD, ng/mL	3.00±3.53	2.39±3.27	0.667
Ferritin, mL/ng	569.25±354.21	611.42±468.71	0.822
Fibrinogen, mg/dL	5.77±2.23	4.48±2.33	0.257
INR	1.00±0.08	1.07±0.17	0.292
Procalcitonin, ng/mL	1.62±3.76	4.49±14.15	0.605

ADAMTS13: A Thrombospondin Type-1 Motif, Member 13, HGB: Hemoglobin, Lym: Lymphocyte, Neu: Neutrophil, PLT: Trombocyte, WBC: White blood cell count, ALT: Alanine aminotransferase, AST: Aspartate aminotransferase, CRP: C-reactive protein, DD: D-Dimer, INR: International normalized ratio

Rheumatology Quarterly 2024;2(3):137-43

Aydın et al. ADAMTS13 Levels in COVID-19 Patients

Table 6. Variation in parameters among COVID patients without lung involvement depending on the presence or absence of chronic disease

	Chronic disease is absent (n=17)	Chronic disease is present (n=13)	p-value
ADAMTS13, ng/mL	0.84±0.62	1.01±0.52	0.400
Age	53.55±14.55	62.62±14.42	0.089
Clinical hospitalization days	4.50±4.38	3.15±3.28	0.367
Symptom duration	7.25±2.95	6.23±2.16	0.309
HGB, gr/dL	14.16±1.44	13.10±2.09	0.119
Lym, $10^3/\mu L$	1.21±0.53	1.05±0.60	0.444
PLT, $10^3/\mu L$	189.63±35.40	181.92±72.66	0.711
WBC, $10^3/\mu L$	5.38±2.86	4.831.72	0.544
AST, µ/L	32.73±12.84	31.63±16.49	0.844
ALT, µ/L	32.00±16.88	22.96±11.18	0.121
CRP, mg/dL	27.55±24.91	32.57±37.15	0.672
DD, ng/mL	0.76±0.36	0.84±0.64	0.824
Ferritin, mL/ng	275.00±204.16	172.14±125.53	0.303
Fibrinogen, mg/dL	4.56±1.33	4.80±0.66	0.710
INR	1.06±0.08	0.99±0.05	0.204

ADAMTS13: A Thrombospondin Type-1 Motif, Member 13, HGB: Hemoglobin, Lym: Lymphocyte, PLT: Trombocyte, WBC: White blood cell count, ALT: Alanine aminotransferase, AST: Aspartate aminotransferase, CRP: C-reactive protein, DD: D-Dimer, INR: International normalized ratio

intensive care and received pulse steroid therapy according to the Ministry of Health regulations.

In various studies, high rates of venous thrombotic events have been observed in patients with SARS-CoV-2. In China, venous thrombosis was reported at a rate of 25% in a group of 81 patients who were not treated with routine thromboprophylaxis (14). In a study by Middeldorp et al. (15), venous thrombosis was detected in 35 of 75 intensive care unit patients who received thrombosis prophylaxis. In addition, coagulopathy and abnormal coagulation parameters can lead to increased mortality (16). For all these reasons, it is important to recognize the etiology of thrombosis in patients with SARS-CoV-2 to reduce mortality.

SARS-Cov-2 infects the pulmonary excess alveolar epithelium and subsequently the endothelium via the angiotensin-converting enzyme 2 (ACE-2) receptor. vWF multimers are released from damaged endothelium, leading to excessive cytokine release develops. Because the virus enters the cell via ACE-2, ACE-2 deficiency develops and angiotensin 1-7 is reduced (anti-thrombotic, anti-inflammatory, anti-fibrotic, vadodilator and reactive oxygen species neutralizer). Hyperinflammation predominates in the proinflammatory and prothrombotic phases, resulting in the release of vWF, decreases in angiotensin 1-7, and hyperinflammation leading to the development of thrombosis (17-19).

Excessive vWF release from damaged endothelium may decrease the amount of ADAMTS13 due to depletion. Neutrophil extracellular traps (NETs) are active in the COVID-19 prothrombotic phase. Various stimuli such as bacteria, fungi, viruses, parasites, activated platelets, and certain chemicals can induce NET formation, which is known as NETosis. NETs are composed of DNA, histones, and proteins, as well as neutrophil elastase (NE), myeloperoxidase, cathepsin G, proteinase 3, metalloproteinase 9, and human neutrophil peptide 1. In NETosis, ADAMTS13 is inactivated by NE and other proteases and its levels are decreased (20-22).

In addition, IL-8, TNF-α, and IL-6 stimulate the release of ultra-large vWF multimers, leading to the formation of platelet arrays under flow conditions, and IL-6 prevents ADAMTS13 from cleaving vWF. It is known that IL-6 levels are elevated in patients diagnosed with COVID-19. In our study, the significantly lower ADAMTS13 level in the outpatient COVID-19 group compared to the control group may be due to an increase in the amount of vWF due to IL-6 release and a decrease in ADAMTS13 as a result of consumption (22-24). Similar to our study, another study showed that ADAMTS13 activity decreased in COVID-19 patients (25).

Aydın et al. ADAMTS13 Levels in COVID-19 Patients

Rheumatology Quarterly 2024;2(3):137-43

In addition, another study reported a relative decrease in ADAMTS13 levels (26). Martinelli et al. (27) found an increase in D-Dimer levels in patients with SARS-CoV-2, an inverse correlation between D-Dimer levels and ADAMTS13 levels, and a relative decrease in ADAMTS13 levels, although not statistically significant.

In our study, the ADAMTS13 level was lower in the COVID-19 group without lung involvement than in the control group. The decreased expression of ADAMTS13 may be explained by disease-specific mechanisms and mechanisms observed in other infections and inflammations.

In Disseminated Intravascular Coagulopathy (DIC), tissue factor expression increases and microthrombus formation is observed as a result of excessive cytokine release, supporting the hypothesis that cytokine increase decreases ADAMTS13 levels. Proteases such as thrombin and plasmin degrade ADAMTS13 in DIC and decrease its amount. Mancini et al. (28) showed that ADAMTS13 levels decreased with increasing lung involvement. Similarly, in our study, ADAMTS13 levels were lower in the group with lung involvement than in the control and non-lung involvement.

One study showed that α1-antitrypsin treatment was effective in preventing the appearance of unusually large vWF multimers in the circulation, but not in preventing TTP recurrence. This suggests that granulocyte elastase cleaves ADAMTS13, thereby reducing its activity and quantity. In other words, in sepsis, proteases may degrade ADAMTS13 and reduce its activity and quantity (29).

Antibodies against ADAMTS13 are known. This condition is defined as the cause of acquired TTP in patients with TTP. Binding of autoantibodies to ADAMTS13 either inhibits ADAMTS13 activity or induces clearance of the resulting immunocomplexes. As a result, the number of ADAMTS13 decreases, vWF multimers increase in the circulation, and ADAMTS13 immunocomplexes with reduced activity appear. As a result, there is a predisposition to thrombosis (30,31).

Study Limitations

In our study, the limitation of the study was that the ADAMTS13 level was not measured before pulse steroid treatment in patients with COVID-19 and lung involvement. The change in ADAMTS13 level according to the level of lung involvement was not studied, and the ADAMTS13 activity was not assessed. In addition, the statistically significant difference in age between the control and patient groups was a limitation of our study

CONCLUSION

In our study, the significant decrease in ADAMTS13 levels in the COVID-19 group without lung involvement indicates that there may be a predisposition to thrombosis even in the initial stage of COVID-19 and in mild cases without lung involvement. This picture calls into question the necessity of anti-thrombotic therapy even in mild cases of COVID-19. In patients with lung involvement, ADAMTS13 levels were lower than those without lung involvement, indicating that lung involvement in COVID-19 patients may increase susceptibility to thrombosis. In addition, the lower ADAMTS13 levels in patients who died, although not significant, suggests that the decrease in ADAMTS13 levels indicates that the prognosis will worsen. There are many examples of the mechanism of thrombosis development in patients with COVID-19. The use of steroids may reduce the development of thrombosis by suppressing the inflammatory and immunologic pathways. The use of vWF antibodies, IL-1, and IL-6 antibodies, or recombinant ADAMTS13 as novel treatment strategies may reduce thrombosis, and new studies are needed in this respect.

Footnote

Authorship Contributions

REFERENCES

1. World Health Organization (WHO). Who weekly epidemiological update-20 October 2020. Data as received by WHO from national authorities, as of 18 October 2020, 10 am CEST, 2020. https://www.who.int/docs/default-source/coronaviruse/situation-reports/20201020-weekly-epi-update-10.pdf?sfvrsn=58786643_26&download=true

Rheumatology Quarterly 2024;2(3):137-43

Aydın et al. ADAMTS13 Levels in COVID-19 Patients

2. Bhatraju PK, Ghassemieh BJ, Nichols M, et al. Covid-19 in critically Ill patients in the Seattle Region-case series. N Engl J Med. 2020;382:2012-22.

3. Wiersinga WJ, Rhodes A, Cheng AC, et al. Pathophysiology, transmission, diagnosis, and treatment of Coronavirus Disease 2019 (COVID-19): A review. JAMA. 2020;324:782-93.

4. Islam KU, Iqbal J. An update on molecular diagnostics for COVID-19. Front Cell Infect Microbiol. 2020;10:560616.

5. Helms J, Tacquard C, Severac F, et al. High risk of thrombosis in patients with severe SARS-CoV-2 infection: a multicenter prospective cohort study. Intensive Care Med. 2020;46:1089-98.

6. Franchini M, Marano G, Cruciani M, et al. COVID-19-associated coagulopathy. Diagnosis. 2020;7:357-63.

7. Turner NA, Nolasco L, Ruggeri ZM, et al. Endothelial cell ADAMTS-13 and VWF: production, release, and VWF string cleavage. Blood. 2009;114:5102-11.

8. Diz-Küçükkaya R. ADAMTS-13 ve trombotik mikroanjiopatiler. Türk Hematoloji Derneği. 23-26 Ekim 2013, Antalya. https://www.thd.org.tr/thdData/Books/679/adamts-13-ve-trombotik-mikroanjiopatiler-reyhan-diz-kucukkaya.pdf

9. Rieger M, Ferrari S, Kremer Hovinga JA, et al. Relation between ADAMTS13 activity and ADAMTS13 antigen levels in healthy donors and patients with thrombotic microangiopathies (TMA). Thromb Haemost. 2006;95:212-20.

10. Cao WJ, Niiya M, Zheng XW, et al. Inflammatory cytokines inhibit ADAMTS13 synthesis in hepatic stellate cells and endothelial cells. J Thromb Haemost. 2008;6:1233-5.

11. Zheng XL. ADAMTS13 and von Willebrand factor in thrombotic thrombocytopenic purpura. Annu Rev Med. 2015;66:211-25.

12. T.C. Sağlık Bakanlığı Halk Sağlığı Genel Müdürlüğü. COVID-19 (SARS-CoV-2 Enfeksiyonu) erişkin hasta tedavisi. 12 Ekim 2020. https://covid19.saglik.gov.tr/Eklenti/39061/0/covid-19rehberieriskinhastatedavisipdf.pdf

13. T.C. Sağlık Bakanlığı Halk Sağlığı Genel Müdürlüğü. COVID-19 (SARS-CoV-2 Enfeksiyonu) Ağır pnömoni, ARDS, sepsis ve septik şok yönetimi. 7 Kasım 2020. https://covid19.saglik.gov.tr/Eklenti/39297/0/covid19rehberiagirpnomoniardssepsisveseptiksokyontemipdf.pdf

14. Cui S, Chen S, Li X, et al. Prevalence of venous thromboembolism in patients with severe novel coronavirus pneumonia. J Thromb Haemost. 2020;18:1421-4.

15. Middeldorp S, Coppens M, van Haaps TF, et al. Incidence of venous thromboembolism in hospitalized patients with COVID-19. J Thromb Haemost. 2020;18:1995-2002.

16. Levi M, Scully M. How I treat disseminated intravascular coagulation. Blood. 2018;131:845-54.

17. Lee C, Choi WJ. Overview of COVID-19 inflammatory pathogenesis from the therapeutic perspective. Arch Pharm Res. 2021;44:99-116.

18. Domingo P, Mur I, Pomar V, et al. The four horsemen of a viral Apocalypse: The pathogenesis of SARS-CoV-2 infection (COVID-19). EBioMedicine. 2020;58:102887.

19. Sweeney JM, Barouqa M, Krause GJ, et al. Evidence for secondary thrombotic microangiopathy in COVID-19. medRxiv [Preprint]. 2020:2020.10.20.20215608.

20. Laridan E, Martinod K, De Meyer SF. Neutrophil extracellular traps in arterial and venous thrombosis. Semin Thromb Hemost. 2019;45:86-93.

21. Fuchs TA, Bhandari AA, Wagner DD. Histones induce rapid and profound thrombocytopenia in mice. Blood. 2011;118:3708-14.

22. Yang J, Wu Z, Long Q, et al. Insights into immunothrombosis: The interplay among neutrophil extracellular trap, von Willebrand factor, and ADAMTS13. Front Immunol. 2020;11:610696.

23. Coomes EA, Haghbayan H. Interleukin-6 in Covid-19: A systematic review and meta-analysis. Rev Med Virol. 2020;30:1-9.

24. Levine SJ, Larivée P, Logun C, et al. Corticosteroids differentially regulate secretion of IL-6, IL-8, and G-CSF by a human bronchial epithelial cell line. Am J Physiol. 1993;265:L360-8.

25. Ward SE, Fogarty H, Karampini E, et al. ADAMTS13 regulation of VWF multimer distribution in severe COVID-19. J Thromb Haemost. 2021;19:1914-21.

26. Martín-Rojas RM, Chasco-Ganuza M, Casanova-Prieto S, et al. A mild deficiency of ADAMTS13 is associated with severity in COVID-19: comparison of the coagulation profile in critically and noncritically ill patients. Blood Coagul Fibrinolysis. 2021;32:458-67.

27. Martinelli N, Montagnana M, Pizzolo F, et al. A relative ADAMTS13 deficiency supports the presence of a secondary microangiopathy in COVID 19. Thromb Res. 2020;193:170-2.

28. Mancini I, Baronciani L, Artoni A, et al. The ADAMTS13-von Willebrand factor axis in COVID-19 patients. J Thromb Haemost. 2021;19:513-21.

29. Galbusera M, Ruggenenti P, Noris M, et al. alpha 1-Antitrypsin therapy in a case of thrombotic thrombocytopenic purpura. Lancet. 1995;345:224-5.

30. Joly BS, Coppo P, Veyradier A. Thrombotic thrombocytopenic purpura. Blood. 2017;129:2836-46.

31. Plášek J, Gumulec J, Máca J, et al. COVID-19 associated coagulopathy: Mechanisms and host-directed treatment. Am J Med Sci. 2022;363:465-75.

DIGITAL ULCERATION FOLLOWING GEMCITABIN PLUS CISPLATIN CHEMOTHERAPY IN A SYSTEMIC SCLEROSIS PATIENT WITH LUNG ADENOCARCINOMA

Ⓘ Hüseyin Oruç, Ⓘ Reşit Yıldırım, Ⓘ Nazife Şule Yaşar Bilge, Ⓘ Timuçin Kaşifoğlu

Eskişehir Osmangazi University Faculty of Medicine, Department of Internal Medicine, Clinic of Rheumatology, Eskişehir, Turkey

Abstract

Systemic sclerosis (SSc) is a systemic autoimmune disease characterized by fibrosis and vascular dysfunction in the skin and visceral organ systems. Digital ulceration is one of the major cause of morbidity. Although its pathogenesis has not been fully elucidated, structural and functional disturbances in small vessels are considered one of the major mechanisms. While cold exposure is considered the most important inciting factor for the development of digital ulceration, drugs and physical trauma are other described triggering factors. Herein, we report a case with SSc diagnosis who developed digital ulcers following gemcitabine and cisplatin chemotherapy for lung adenocarcinoma.

Keywords: Systemic sclerosis, vasculopathy, chemotherapy, digital ulceration, management

INTRODUCTION

Systemic sclerosis (SSc) is a systemic autoimmune disease characterized by fibrosis and vascular dysfunction in the skin and visceral organ systems. Digital ulceration is a significant organ involvement related to morbidity. Many hypotheses have been proposed for the development of digital ulceration; however, structural and functional disturbances in small vessels are considered major mechanisms (1,2). Additionally, there are disease-related and environmental factors (including drugs) that contribute to the development of digital ulceration. Here, we describe a case of a patient with a previous diagnosis of SSc who presented with digital ulceration in both hands shortly after receiving gemcitabine and cisplatin chemotherapy for lung adenocarcinoma. Our aim in this report is to draw attention to this issue and discuss management strategies in light of the literature.

CASE REPORT

A 48 year old female was admitted to the hospital with a new onset painful ulceration at the tip of both hands. She reported that this condition started suddenly five days ago and deteriorated in the last 3 days. Past medical history showed that she was diagnosed with SSc five years ago based on the presence of Raynaud's phenomenon, bilateral sclerodactyly, telangiectasis, lung involvement (non-specific interstitial pneumonia) and high titers of anti-nuclear antibody (1/640-

1/1000) and Scl-70 positivity (4+). She was treated with cyclophosphamide and glucocorticoids for lung involvement. After completion of four cycles of cyclophosphamide, steroid was stopped at one month and maintainance treatment with azathioprine (100 mg/day) commenced as her lung parencyhma responded well to induction therapy with no symptoms of dyspnea and showed radiologic improvement on chest computed tomography (CT) control at month four of follow-up. During follow-up every three to six months under azathioprine, nifedipine, acetylsalicilic acid and lansoprazole for SSc, a cavitary lung mass was incidentally detected by CT imaging of the chest for routine control of lung involvement three years after SSc diagnosis. Positron emission tomography (PET)-CT imaging was consistent with metastatic malignancy, however, the initial biopsy examination was noncontributory. After surgical excision, histopathologic examination confirmed the diagnosis of undifferentiated adenocarcinoma of the lung (PDL-1 negative and c-Erb2 positive). After unresponsiveness to combination of carboplatine and paclitaxel as the first line treatment, pemethrexed was given, but the cancer progressed. Thus, nivolumab was started, however, the drug was cessated shortly after due to drug intolerance. Lastly, combination of gemcitabine and cisplatine administered three months ago. Treatment was well-tolerated and lung mass decreased in size, however, ten days after the third cycle (10 days following gemcitabine), she presented with painful digital ulceration (Figure 1). She reported no recent infection and physical trauma. Physical examination showed necrotic digital ulcers at the tip of both hands. Radial pulses were palpable bilaterally. Modified Rodnan Skin Score was calculated 6 and lung examination was noncontributory. Microbiologic examination revealed no organisms. Thrombocyte counts, fibrinogen and D-dimer levels were normal but mild elevation in c-reactive protein (10 mg/dL; reference 0-5) was found. Doppler ultrasound imaging showed intact radial and ulnar pulses in upper extremities. During the whole cancer treatment period, no evidence of SSc organ progression was observed in terms of skin, lung and other organs. Skin scores were similar and chest CT imaging until detection of lung mass did not suggest any progression in SSc related lung involvement. After excluding these possibilities, the new onset digital ulceration was attributed to gemcitabine plus cisplatine chemotherapy. The patient was recommended for hospitalization to initiate intravenous iloprost, but she refused due to family reasons. Her nifedipine dose escalated to maximally tolerated dose (120 mg/day) and pentoxyphylline was added to acetylsalicylic acid. Moreover, she was consulted with the oncology department regarding the current complication. Gemcitabine plus cisplatine combination was replaced with

another regimen as benefits overweigh risks. At one month follow-up visit, her lesions showed total recovery (Figure 1). She is currently on nifedipine, pentoxyphylline and acetylsalicylic acid for SSc and under chemotherapy for her metastatic cancer.

DISCUSSION

Digital ulceration in SSc remains a major problem in clinical practice. The primary pathogenesis is considered to be alterations in the vasculature of extremities. Vasculopathy in SSc consists of endothelial dysfunction, defective angiogenesis, and altered vasculogenesis (2). While environmental factors such as persistent exposure to cold weather are major determinants of ulcer development, other causes have also been described, including trauma, thrombosis, and drugs (2). Notably, serious thrombotic complications in various organs have been reported in patients after gemcitabine plus platinum-based regimens, mainly associated with increased cumulative doses (3). Digital ulceration and necrosis have also been reported following gemcitabine in SSc patients (4,5). Indeed, in our case we can not ignore the possiblity of that this incident might occur as solely

Figure 1. A) Digital ulcerations at the fingertips tip and at the edges of the nails, B) Follow-up examination at 1 month revealed fully recovered lesions

Oruç et al. Digital Ulceration Induced by Chemotherapy

Rheumatology Quarterly 2024;2(3):144-6

disease related, which can be considered as a limitiation however, recent usage of these agents and no SSc related vascular events for a long time are supporting that there is a strong relationship between these agents and the incident.

It is well known that SSc patients have endothelial dysfunction and a microvascular environment sensitive to hypoxia, procoagulant activity, and external stimuli. This microenvironment might explain the contribution of gemcitabine and cisplatin in developing digital ulceration in our case. Management includes intravenous prostacyclin analogues, calcium channel blockers, and other vasodilators, as well as wound care and prevention of infectious complications (3). Moreover, there is no consensus on prophylaxis in those maintaining their same anti-cancer regimens. It is of great importance that physicians are aware that gemcitabine and cisplatin might increase the tendency for microvascular thrombotic complications in SSc patients. The cessation and/or continuation of cancer drugs should be tailored in collaboration with the oncology department according to the activities and benefits of both diseases.

CONCLUSION

SSc patients are prone to developing vascular complications, leading to digital ulcerations. Potential risk factors should be minimized for better outcomes. Clinicians should keep in mind that some chemotherapeutic agents can induce vasculopathy in this population if cancer is concomitantly present. In the case of a chemotherapy-related vascular event in an SSc patient, treatment should be discussed with oncology with the patient's best interest in mind.

REFERENCES

1. Volkmann ER, Andréasson K, Smith V. Systemic sclerosis. Lancet. 2023;401:304-18.

2. Truchetet ME, Brembilla NC, Chizzolini C. Current concepts on the pathogenesis of systemic sclerosis. Clin Rev Allergy Immunol. 2023;64:262-83.

3. Dasanu CA. Gemcitabine: vascular toxicity and prothrombotic potential. Expert Opin Drug Saf. 2008;7:703-16

4. Clowse ME, Wigley FM. Digital necrosis related to carboplatin and gemcitabine therapy in systemic sclerosis. J Rheumatol. 2003;30: 1341-3.

5. So E, Crees ZD, Crites D, et al. Digital ischemia and necrosis: a rarely described complication of gemcitabine in pancreatic adenocarcinoma. J Pancreat Cancer. 2017;3:49-52.